DOT/TSC-RA-3-8-2

Project Report
ATC-26
Vol. II

Technical Assessment of Satellites for CONUS Air Traffic Control

Volume II: Random Access Aircraft-to-Satellite Techniques

K.S. Schneider
R.S. Orr

28 February 1974

Lincoln Laboratory
MASSACHUSETTS INSTITUTE OF TECHNOLOGY
LEXINGTON, MASSACHUSETTS

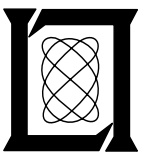

Prepared for the Transportation Systems Center.

TECHNICAL REPORT STANDARD TITLE PAGE

1. Report No.	2. Government Accession No.	3. Recipient's Catalog No.
DOT/TSC-RA-3-8-2		

4. Title and Subtitle	5. Report Date
Technical Assessment of Satellites for CONUS Air Traffic Control. Vol. II: Random Access Aircraft-to-Satellite Techniques	28 February 1974
	6. Performing Organization Code

7. Author(s)	8. Performing Organization Report No.
K. S. Schneider and R. S. Orr	ATC-26 Vol. II

9. Performing Organization Name and Address	10. Work Unit No.
Massachusetts Institute of Technology Lincoln Laboratory P. O. Box 73 Lexington, Massachusetts 02173	11. Contract or Grant No. DOT/TSC-RA-3-8
	13. Type of Report and Period Covered Project Report
12. Sponsoring Agency Name and Address Transportation Systems Center Department of Transportation 55 Broadway Cambridge, Massachusetts 02142	14. Sponsoring Agency Code

15. Supplementary Notes

The work reported in this document was performed at Lincoln Laboratory, a center for research operated by Massachusetts Institute of Technology.

16. Abstract

A number of satellite system techniques have been suggested as candidates to provide ATC surveillance, communication, and/or navigation service over CONUS. All techniques perform position determination by multilateration using a constellation of satellites. They can be categorized as follows: 1) Coordinated Aircraft-to-Satellite Techniques (CAST), 2) Random Access Aircraft-to-Satellite Techniques (RAST), 3) Satellite-to-Aircraft Techniques (SAT). A technical assessment is made of the various techniques with no one particular technique emerging as superior; several feasible alternatives are identified. The assessment indicates that satellite based techniques for CONUS ATC can be developed without relying on high risk technology.

This volume deals with RAST; CAST and SAT are treated in companion volumes. A system employing RAST could operate by having each aircraft transmit a unique signature periodically, without any coordination of transmissions. The position of an aircraft is then obtained by multilateration using the arrival times of its signature at four or more satellites. Since aircraft transmissions are not coordinated, there is the possibility that different signatures may overlap at a satellite receiver. The resulting mutual interference is a factor in the performance of systems employing RAST. The critical technical aspects of RAST are explored with special emphasis on signaling formats, satellite coverage issues, degradation due to mutual interference and susceptibility to jamming.

17. Key Words	18. Distribution Statement
Air Traffic Control surveillance satellite systems AATMS	Document is available to the public through the National Technical Information Service, Springfield, Virginia 22151.

19. Security Classif. (of this report)	20. Security Classif. (of this page)	21. No. of Pages	22. Price
Unclassified	Unclassified	110	4.25 HC 1.45 MF

Form DOT F 1700.7 (8-69)

TABLE OF CONTENTS

CONTENTS (Continued)

CONTENTS (Continued)

LIST OF ILLUSTRATIONS

ILLUSTRATIONS (Continued)

LIST OF TABLES

SECTION 1

INTRODUCTION AND SUMMARY OF CONCLUSIONS

1.1 OVERVIEW OF SATELLITE SYSTEM TECHNIQUES

Over the last half decade a number of satellite system techniques have been advanced as candidates to provide Air Traffic Control (ATC) surveillance, communication and/or navigation service over the CONtinental United States (CONUS).[1-7] Each technique has its advantages and disadvantages. All employ position determination service by multilateration using a constellation of satellites. These techniques can be grouped into three basic categories based on certain key technical features. The three categories are:

Coordinated Aircraft-to-Satellite Techniques (CAST)

> Systems employing these techniques interrogate aircraft sequentially. The response from an aircraft is the transmission of a timing pulse. This pulse is received by the satellites and then relayed to a ground processing facility. The ground processing facility determines the signal time of arrival (TOA) at each of the satellites and estimates the aircraft position by multilateration. The position information is then incorporated into the ATC surveillance data base. The interrogation algorithm is designed to eliminate overlapping signal pulses at the satellites and hence mutual interference.

Random Access Aircraft-to-Satellite Techniques (RAST)

> Systems employing these techniques have each aircraft transmit a timing pulse which is received by four or more satellites and relayed to a ground processing facility. This facility determines TOA at each of the satellites and estimates the aircraft position by hyperbolic multilateration. The position information is then incorporated into the ATC surveillance data base. Since aircraft transmit in an uncoordinated manner, system performance, i.e. accuracy and update rate, is ultimately limited by mutual interference caused by signal overlap at satellite receivers.

Satellite-to-Aircraft Techniques (SAT)

> Systems employing these techniques operate by having four or more satellites periodically transmit timing pulses to aircraft. A navigation processor (computer) aboard each aircraft determines the aircraft position from the signal TOA's. The information also can be data linked to the ground for inclusion in a ground maintained ATC surveillance data base.

This volume is concerned with an assessment of the critical technical aspects of Random Access Aircraft-to-Satellite Techniques (RAST). The other two techniques are treated in Volumes I and III.[8,9]

These three volumes concentrate only on the crucial technical issues. They do not attempt to assess the broad spectrum of operational or economic implications of employing these techniques in the National Airspace System. Issues such as the cost-effectiveness of satellites as an element in the CONUS ATC system are beyond the scope of these investigations. Detailed questions concerning the manner by which any of these satellite techniques might evolve from present day aircraft surveillance/navigation systems are also outside the scope of this report. Detailed operational requirements that would be imposed upon a satellite system for CONUS ATC have not been given consideration in depth.

The results of the technical assessment of all three satellite techniques have verified that satellite-based techniques for CONUS ATC could be developed without reliance on high risk technology. No one particular technique has emerged as superior; rather, several feasible alternatives have been identified.

One of the primary attractive attributes of satellites is their inherent ability to provide broad coverage of low altitude airspace. Unpressurized general aviation aircraft are predominant users of low altitude airspace.

Hence, a central issue is the complexity of general aviation avionics required for satellite operation. It has been concluded that all three of the techniques considered require more sophisticated avionics (for a given user class) than is currently employed for comparable service with today's ground based system.

1.2 RANDOM ACCESS AIRCRAFT-TO-SATELLITE TECHNIQUES (RAST)

With RAST, each participating aircraft is assumed to periodically transmit a uniquely identifying signature waveform to a constellation of satellites. These transmissions are relayed to a ground station where they are used to establish both the presence of the aircraft and to determine its position. RAST is distinguished from CAST in that for the former the aircraft transmissions are mutually uncoordinated and the possibility arises that signature receptions will overlap in time at satellite receivers. The effects of this mutual interference cannot be ignored in a performance assessment of RAST.

Successful operation of a system employing RAST is contingent upon its ability to both acquire and track aircraft. Because of the importance of the acquisition/tracking performance, these issues have been studied in some depth.

1.3 PRINCIPAL CONCLUSIONS

As a result of the study reported herein, a number of conclusions can be drawn. These conclusions pertain principally to the technological feasibility of RAST.

A. NO IMPENETRABLE TECHNOLOGICAL BARRIERS PRECLUDE THE FEASIBILITY OF EMPLOYING RANDOM ACCESS AIRCRAFT-TO-SATELLITE TECHNIQUES.

The satellite and avionics technologies which are pertinent to these techniques appear to be well within present day capabilities. Consequently, the feasibility is not contingent upon any high risk technological advance.

B. HIGH GAIN SATELLITE ANTENNAS ARE DICTATED BY THE DESIRE FOR LOW COST AVIONICS WHICH ARISES FROM THE INCLUSION OF GENERAL AVIATION IN THE SYSTEM.

Among the numerous alternatives for the realization of a system which employs RAST, certain ones are strongly preferred with regard to the inclusion of general aviation aircraft with low cost avionics. Specifically, by employing a large, high gain, narrow beamwidth antenna rather than a small, moderate gain, CONUS coverage antenna for each satellite, the need for high peak output power at the aircraft transmitter is diminished. Such an antenna must utilize several beams in order to maintain CONUS coverage. Since coverage regions are neither mutually exclusive nor identical from different satellite positions, care must be exercised in exploiting this capability.

C. A HIGH GAIN SATELLITE ANTENNA PROVIDES AN EFFECTIVE WAY TO REDUCE THE EFFECT OF THE MUTUAL INTERFERENCE CAUSED BY THE UNCOORDINATED (AND SOMETIMES OVERLAPPING) AIRCRAFT TRANSMISSIONS.

In systems employing RAST which use a single beam CONUS coverage satellite antenna, transmissions from aircraft anywhere in CONUS can mutually interfere. However, in systems which use a high gain multiple beam antenna to provide CONUS coverage, mutual interference occurs only among aircraft within the same beam.

D. THE REQUIRED AVIONICS COMPLEMENT IS SIGNIFICANTLY MORE COMPLEX (AND COSTLY TODAY) THAN THE CORRESPONDING ATCRBS AVIONICS.

For adequate ranging accuracy, coherent pulse transmitters are required. To limit the disadvantage of any one user relative to the fleet, careful power monitoring is essential, i.e., transmitters ideally should have identical ERP's. The contrast with ATCRBS transponders (with their 6-8.5 dB power tolerance, 3 MHz frequency tolerance and incoherent short pulse operation) is evidence of the high complexity of the avionics required in systems which employ RAST. Despite the fact that for basic surveillance service with RAST no aircraft receiver is required, the complexity of the transmitter is expected to result in an avionics cost higher than that of today's ATCRBS transponder.

E. COMMONALITY OF EQUIPMENT WITH UPGRADED THIRD GENERATION ATC AVIONICS CANNOT SUPPORT SUBSTANTIAL SAVINGS IN THE TOTAL AVIONICS COST.

Total avionics cost could in principle be decreased by exploiting commonality among onboard equipment. However, the necessity for upper-hemispherical coverage, operation in the 1535-1660 MHz allocation and coherent transmission provides little opportunity for appreciable savings through integration with other avionics planned for the Upgraded Third Generation System.

F. A LARGE CENTRALIZED DATA PROCESSING FACILITY REQUIRING THE COORDINATED EFFORTS OF AT LEAST SEVERAL TENS OF PRESENT DAY GENERAL PURPOSE CPU'S AND FAST RANDOM ACCESS STORAGE IS NEEDED TO CONTROL THE SYSTEM. RELIABLE HARDWARE AND SOFTWARE ENGINEERING FOR SUCH A FACILITY IS A DIFFICULT BUT FEASIBLE GOAL.

The data rates at the ground in this type of system are such that a large amount of simultaneous processing is required for filtering and position

determination. Rapid random access (possibly precluding disc and drum storage) to data is also required. All told, these processing requirements are more demanding than those of, for example, NAS Stage A.

G. SYSTEMS EMPLOYING RAST ARE VULNERABLE TO FAILURE OF THEIR CENTRAL PROCESSING FACILITY AND TO THREATS FROM A TERRESTRIAL JAMMER.

The facility required to execute the computational functions must be centralized. As such, operation of the entire system is sensitive to failure of this facility. The aircraft-to-satellite link is vulnerable to threats from terrestrial jammers. Several jammers appropriately located in CONUS and using very inexpensive technology could disable an entire surveillance system which employs RAST.

H. WITH PROPER DESIGN, THE AIRCRAFT HANDLING CAPABILITY OF RAST SHOULD, AT A MINIMUM, SUFFICE TO PROVIDE SERVICE TO 50,000 AIRCRAFT WITH A 10 SECOND POSITION UPDATE PERIOD.

This capacity should be adequate to provide service to the anticipated 1990's trafic in either the enroute environment or the airspace outside the coverage of a ground based system.

1.4 PROGRAM

The program of this volume is as follows. In Section 2 we begin by describing the general operation of a surveillance system which employs RAST. Critical technical issues concerning satellite antennas and signature selection are discussed. Surveillance systems which employ RAST require two primary subsystems; one for acquisition of aircraft and one for tracking aircraft position.

SECTION 2

SYSTEM DESCRIPTION AND DESIGN ALTERNATIVES

In this section,the operation of a surveillance system employing RAST is described. Within the general framework of this description lie many alternatives for the design of such a system. Several of these alternatives, specifically the selection of satellite antenna and signature formats, constitute the basis for a comparative analysis of systems employing RAST. These are discussed in some detail.

2.1 SYSTEM DESCRIPTION

A pictorial representation of a surveillance system employing RAST is shown in Fig. 2.1. Each aircraft transmits its signature waveform to a constellation of satellites. The satellites operate as linear (frequency translation) repeaters which relay the received signatures to one or more ground processing stations. At the ground facility the signals relayed by all visible satellites are processed to determine which aircraft are in the airspace and to track their current position. It is convenient to identify two primary ground processing subsystems; acquisition and tracking.

The acquisition subsystem has as its principal function the detection of aircraft in the airspace. Aircraft so detected are passed on to the tracking subsystem for accurate real time position determination.

It is operationally convenient to view the acquisition subsystem as one which processes the set of received waveforms with a bank of matched filter-envelope detector receivers. These are used to detect the presence of an

The assumed operation of these subsystems is described in Section 3. Section 4 summarizes and compares the performance of several variants of a surveillance system employing RAST. In the final section of this volume, two issues critical to a technical assessment of RAST are considered; the susceptibility to intentional jamming and the complexity of the computation required at the ground facility.

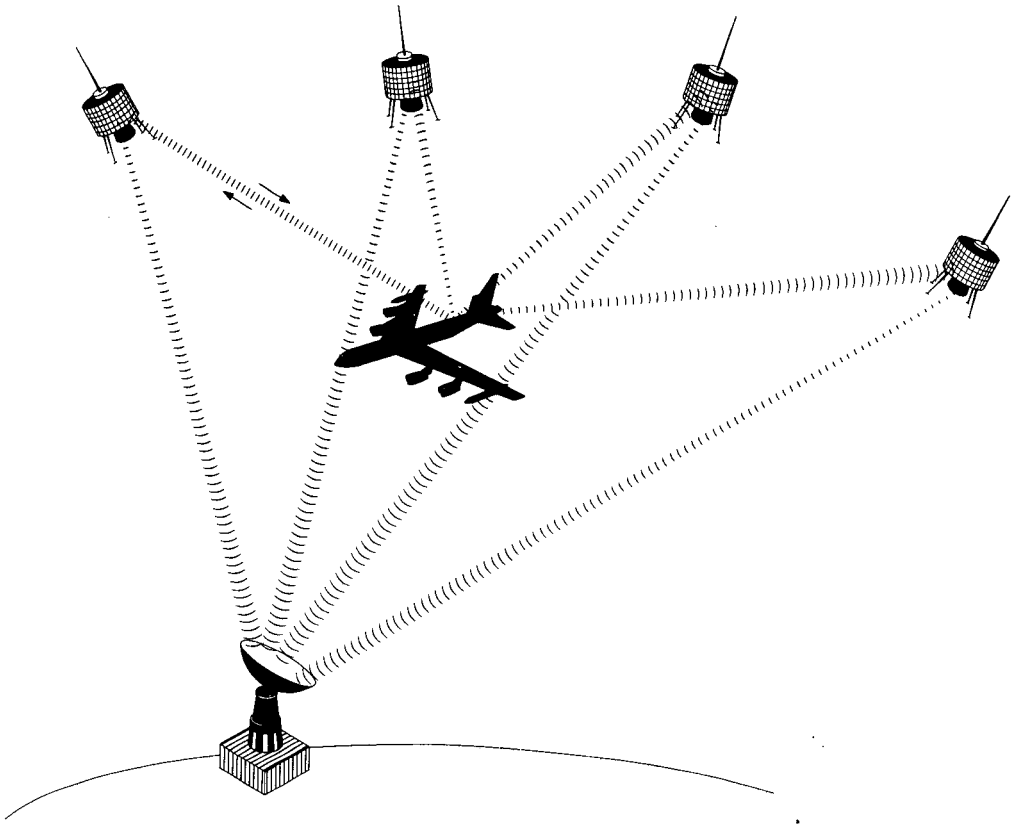

Figure 2.1. ATC Surveillance System Employing RAST.

aircraft signature and to estimate the corresponding signature time of arrival (TOA). In general, sets of aircraft will be searched for sequentially following a search order determined by the a priori likelihood of finding the aircraft in the airspace and the importance of detecting and tracking the aircraft. For example, previously tracked aircraft that have been returned to the acquisition processor for failure to pass a track reliability test or aircraft about to take-off might be given priority in acquisition search. An aircraft is transferred to the tracking processor only after it is satisfactorily acquired. Acquisition requires signature detection by at least four satellites and a resulting set of permissible TOA's. The TOA set is to be considered permissible if the aircraft position computed using the hyperbolic multilateration equations is acceptable. If, for example, the TOA's indicate an aircraft at an altitude of 200,000 ft, they would clearly not be considered permissible.

The tracking subsystem is assumed to have a track file consisting of:

1) a list of detected aircraft currently in the airspace, i.e., those previously detected by the acquisition subsystem and not subsequently returned to it, and

2) the recent past history of the positional data for each such aircraft.

In operation, the tracking subsystem determines position from the set of TOA's for each transmission from every aircraft in its file. It also might use the past history of the positional data of an aircraft to make a velocity estimate. For each transmission the track file is updated by new positional data for the corresponding aircraft. The resulting information can be entered into the appropriate ATC data base.

In RAST, the individual aircraft transmissions are "free-running," i.e., there is no pre-established synchronization or coordination in time among the transmissions of various aircraft. Each aircraft thus has random access to the several satellite uplink channels. The surveillance system must be able to function in the presence of whatever mutual interference is caused by the overlapping arrival of two or more signatures at any of the satellite receivers. This mutual interference (multiple access noise) cannot be ignored in assessing RAST and is, in fact, a major determinant of performance.

2.2 DESIGN ALTERNATIVES

2.2.1 Satellite Antenna Coverage Considerations

In analyzing RAST, we will consider two quite different candidates for the satellite antenna. The first is a single beam antenna having a 10° beamwidth. The beam is broad enough to provide CONUS coverage from synchronous orbit. In a system employing such an antenna, there is little selectivity with respect to angle of arrival at the receiver, and thus signatures must be detected and TOA estimates made in the presence of the mutual interference generated by the transmissions of aircraft anywhere in CONUS. Similar antennas have been assumed in previous studies of RAST.[1]

The second satellite antenna candidate which will be considered has a narrower beamwidth and maintains CONUS coverage by utilizing multiple beams. This antenna is a 30 ft parabolic dish, an example of which is the NASA ATS-F antenna.[10] It has a 1.5° beamwidth and a high (42 dB) gain at a frequency of 1600 MHz. Since mutual interference results primarily from aircraft located within a common beam, the narrow beamwidth of such an antenna serves to

decrease the multiple access noise. The additional antenna gain of this narrow beamwidth antenna will further enhance the received signals relative to receiver noise.

In order to understand how this high gain multibeam antenna could be incorporated effectively into a system employing RAST, it is necessary to determine the coverage provided by the antenna when the satellite is in a variety of orbital positions. This issue is considered in detail in Appendix A for a ten satellite constellation determined by Lee and Wade.[11] The particular constellation has the desirable characteristic of relative insensitivity of position determination accuracy to aircraft orientation, satellite failure and aircraft location. The number of antenna beams required for complete CONUS coverage is shown to vary considerably with satellite orbital position. When the satellite is at a low elevation angle, as few as three beams may suffice for CONUS coverage. The boresight points of the several beams of the antenna must be carefully chosen to avoid significant mutual interference through beam overlap. When the satellite is at a high elevation angle, the number of beams required for CONUS coverage can exceed ten.

In the sequel, we will incorporate various coverage extremes into the analysis of RAST. It should, however, be clearly understood that all assumptions about coverage are consequences of the first order analysis in Appendix A.

2.2.2 Signature Selection Considerations

The signature waveforms used in RAST may be selected in a variety of ways. We have not chosen to investigate the detailed design and/or "optimization" of

signature sets. Rather, for our purposes, we have chosen to concentrate on a particular class of signature sets whose properties are described below.

For our analysis of variants of RAST, attention is restricted to signature waveform sets in which each member signature consists of P equal length non-overlapping pulses selected from a population of N elementary pulses. The interpulse spacing between adjacent pulses is selected from one of I possible values. The maximum number of unique signatures is therefore given by

$$N_{max} = N^P I^{P-1} \tag{2-1}$$

As an example, 10^6 unique signatures could be constructed from P=3 pulses, N=16 possible waveforms and I=16 possible interpulse spacings, i.e.,

$$N_{max} = 16^3 \times 16^2 \simeq 10^6 \tag{2-2}$$

With respect to RAST, the most significant parameters of the signature set are; (1) their time-bandwidth occupancy, (2) the number of unique signatures, (3) the relationship between signature waveform and the accuracy of TOA estimation, and (4) the degree of mutual interference resulting from overlapping arrivals at a receiver. These parameters are principally determined by; (1) the time-bandwidth occupancy of the elementary pulses, (2) the number of elementary pulses (N), signature pulses (P) and interpulse spacings (I), (3) the elementary pulse autocorrelation functions, and (4) the elementary pulse crosscorrelation functions.

Previous investigations of concepts similar to RAST have employed multiple pulse signatures. These signature sets are members of the general class introduced above. When multiple pulse signatures are used, a large number of distinct signatures can be constructed from a small number of elementary pulses (see the example represented by Eq. (2-23)). The small number of pulses can usually be selected to have near optimal auto-and cross-correlation properties.

Signature sets in which each signature consists of a single pulse present a new alternative to the multiple pulse signatures. Both types of signatures will be considered in the subsequent analyses of RAST.

For the purpose of this report, we will consider only binary antipodal phase shift keyed (PSK) pulses with incoherent interpulse phase. Binary on-off keyed pulse amplitude modulation (PAM) is rejected because of the difficulty of constructing pulse sets with good correlation properties from binary waveforms with chip to chip incoherence. It has been shown that good auto- and crosscorrelation properties can be obtained even for the large waveform sets required by single pulse PSK signatures. For example, a set of 10^6 pulses, each composed of 500 PSK chips, can be found having crosscorrelation magnitude less than 0.3, and off peak autocorrelation magnitude less than 0.2.

SECTION 3

ACQUISITION AND TRACKING DESCRIPTION

As a basis for the performance analysis (Section 4) of RAST, the assumed operation of the acquisition and tracking subsystems will be described. This description is intended as a vehicle for the performance analysis, not as an optimized design. Many of the refinements and alternatives which would be investigated in an actual system design are beyond the scope of the present study.

In describing the acquisition and tracking processing, it will be assumed that each aircraft transmits a signature consisting of P pulses; A_1, A_2,...A_p, with interpulse spacings T_1, T_2,...T_{P-1}.* The signature is transmitted periodically every α seconds, the update period. For both acquisition and tracking, the signatures relayed to the ground station are received using matched filter-envelope detectors matched to the individual pulses. Figure 3.1 illustrates a representative signature and Fig. 3.2 illustrates the combined matched filter-envelope detector outputs generated by the signature; in the latter, interference and sidelobes are not shown. The operation of the acquisition and tracking subsystem will be described for a constellation of four visible satellites.

3.1 THE ACQUISITION SUBSYSTEM

When a particular aircraft is to be acquired, retransmissions from each of the four satellites are processed simultaneously. The processing of the signals received from one satellite is executed in the following manner. The

*These should be considered as generic lables for the signature pulses and interpulse spacings.

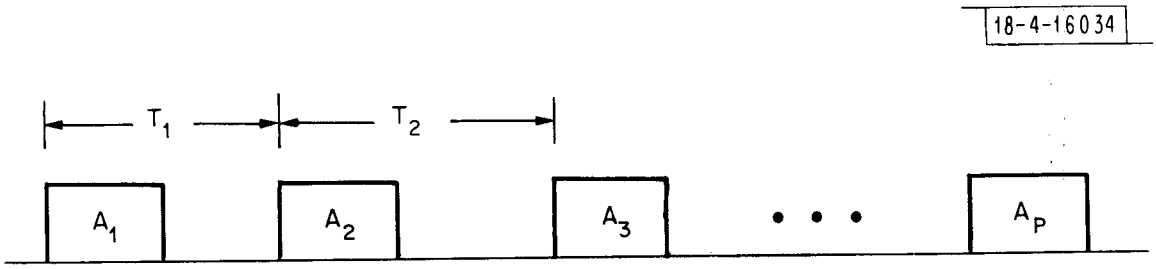

Fig. 3.1. A representative RAST signature.

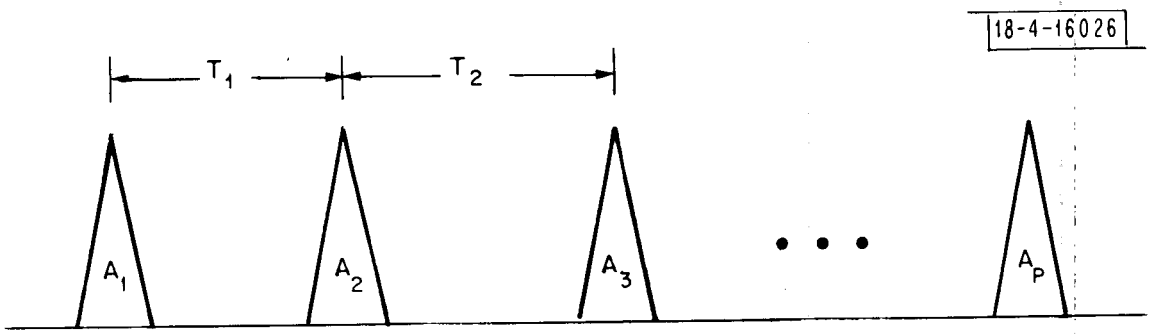

Fig. 3.2. Matched filter-envelope detector outputs corresponding to representative RAST signature.

output of the matched filter-envelope detector corresponding to the aircraft's A_1 pulse is first examined. It is sampled at a rate which exceeds the DPSK chip rate (e.g., at a rate of more than one sample/chip). The samples are threshold tested in order to detect the A_1 pulse. If an A_1 pulse is detected, the time of detection is stored and detections of the subsequent pulses, $A_2,...A_p$, are sought at the outputs of the corresponding matched filter-envelope detectors at the appropriate delays. If all the pulses are found, then this particular aircraft's signature retransmission is declared detected and its time of arrival (TOA) is computed by effectively averaging the P pulse TOA's. During acquisition the pulse TOA is considered as the time at which the pulse is detected.

Regardless of whether or not a signature detection is declared, this processing continues in the same manner for an α second period. The output samples of A_1's envelope detector are first tested, and when required, output samples from the other pulses are tested. Over the α second period this procedure generates a list consisting of all the computed signature arrival times and the corresponding pulse arrival times.

From each of the four individual satellite TOA lists a new list of all possible TOA quadruplets is formed. The aircraft position corresponding to each quadruplet is computed by hyperbolic multilateration and stored with the quadruplets. Ideally, each list will contain only one quadruplet and the position computed from it will be the correct aircraft position. In any case, those positions which are inconsistent with a priori knowledge* about the aircraft are deleted from the list. The first signature TOA quadruplet which is not eliminated from the list is then used to begin a track on the aircraft.

*E.g., general aviation aircraft at 20k ft altitude.

The position corresponding to this TOA quadruplet is supplied to the ATC data base as an acquisition position estimate, and the signature TOA quadruplet is supplied to the tracking subsystem.

3.2 THE TRACKING SUBSYSTEM

The operation of the tracking subsystem can be described inductively. During any given update period, a set of TOA's $\{t_1, t_2, t_3, t_4\}$ corresponding to the reception of a particular aircraft signature is determined. For example, the initial TOA's might be supplied by the acquisition subsystem. These TOA's are used to compute the position of the aircraft and are also used to refine any existing estimate of the aircraft velocity vector. The combination of present aircraft position (equivalently TOA quadruplet), velocity estimate (v), and absolute error in velocity estimate (εv) is used by the tracking subsystem to determine a set of search windows for the next set of signature pulse arrivals. The tracking subsystem searches within these windows for the signature pulses transmitted during the next update period and estimates the TOA's of the next set of signature pulses. Aircraft position during the next update period is then computed from these new TOA estimates and the tracking procedure continues. Following is a more detailed description of this processing.

When a signature TOA estimate is determined, the ground processor assigns an arrival time estimate for the A_j pulse at the i-th satellite; call this time t_i^j. Then, for example, given t_2^1, v and ε, the processor assumes that the A_1 pulse of the signature will be received at satellite 2 in the next update ~~peri~~ period during the uncertainty interval (or window)

$$[t_2^1 + \alpha + \frac{v(1-\varepsilon)\alpha}{c} + \delta_2,\ t_2^1 + \alpha + \frac{v(1+\varepsilon)\alpha}{c} + \delta_2]$$

This situation is illustrated in Fig. 3.3. The parameter δ_2 accounts for satellite motion over an update period; it is a function of the satellite position and orbit and is assumed known at the ground station. The uncertainty interval should be further elongated to account for uncertainties in the estimate of t_i^j, δ_i and ε. Ordinarily, these are negligible compared to $\frac{\varepsilon\alpha v}{c}$, and accordingly, we neglect them in our definition of the uncertainty interval.

The processor determines the peak of the output of A_1's matched filter-envelope detector in this uncertainty interval and notes the time at which this occurs; call this τ_2^1. It takes τ_2^1 as the estimate of the TOA of A_1 at satellite 2 during the next update period.

The same procedure is carried out for the remaining signature pulses. All told, this generates TOA estimates, $\tau_1^1,\ldots\tau_1^p$ for $A_1,\ldots A_p$ during the next update period. Once these estimates have been determined at all four satellites, the TOA differences; $\tau_1^2 - \tau_1^1$, $\tau_1^3 - \tau_1^1,\ldots\tau_1^p - \tau_1^1$, $\tau_2^2 - \tau_2^1,\ldots$ are then compared to the corresponding interpulse spacings of the signature of the aircraft of interest. If one time difference does not correspond to the expected interpulse spacing to within some allowable error (e.g., a few chips), then the tracking of this aircraft terminates and the aircraft is put on the list of aircraft to be reacquired in the next update period.

If the pulse TOA estimates do satisfy the interpulse constraints, a tracking reliability test is performed. As an example, this may be carried out in the following way. For each i=1,...p, the matched filter output samples corresponding to τ_1^i, τ_2^i, τ_3^i, τ_4^i are examined. A threshold test is made on the sample value

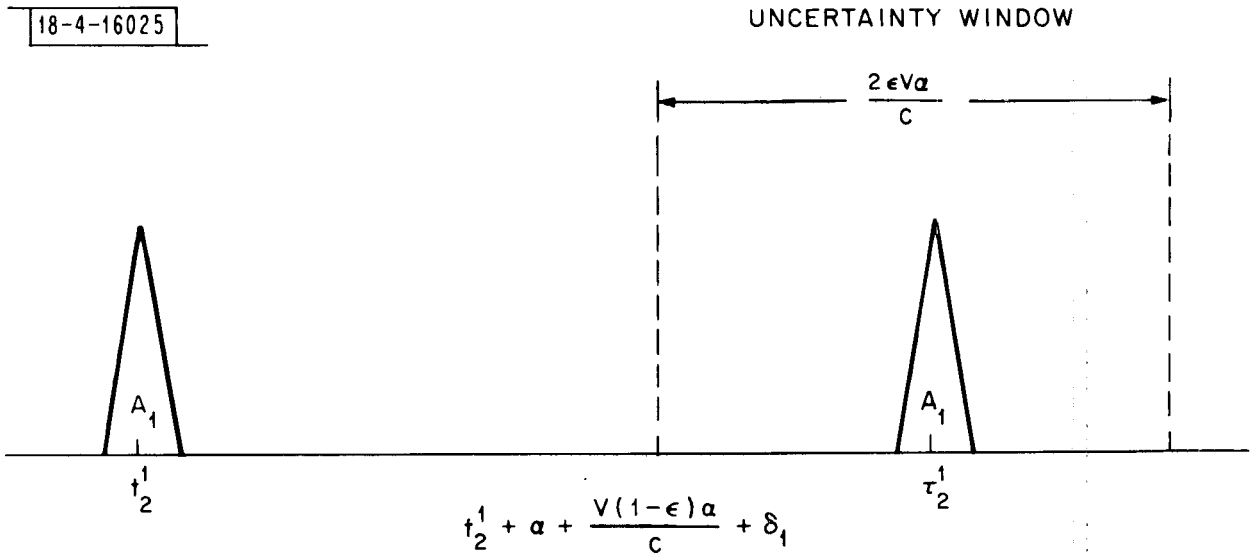

Fig. 3.3. Pulses and uncertainty window in the tracking system.

in order to increase confidence that the maximum was actually generated by the reception of an A_i pulse. If all decisions are affirmative, the track reliability test is passed, otherwise it is failed. If the track reliability test is passed, then the pulse TOA's are averaged to determine an estimate of the signature TOA at each satellite. The resulting quadruplet of signature TOA estimates is used to estimate the aircraft position which is entered into the ATC data base. Because other implementations of this test are possible, the track reliability test is not incorporated into the performance analysis in Section 4.

The velocity estimate, v, used to determine the uncertainty window can be obtained by smoothing past aircraft position data. Immediately after an acquisition period, when there may be little reliable data available, the fractional error ε may be quite large. As the aircraft is tracked, this can be expected to decrease. Table 3.1 indicates the window duration, for several representative values of ε.

TABLE 3.1

UNCERTAINTY INTERVALS FOR VARIOUS AIRCRAFT VELOCITY ASSUMPTIONS

A PRIORI INFORMATION	UNCERTAINTY WINDOW WIDTH
α = 10 sec	
Heading Unknown	
$v \leq$ 1,000 ft/sec	20 μsec
v = 1,000 ± 250 ft/sec (ε=0.25)	5 μsec
v = 1,000 ± 50 ft/sec (ε=0.05)	1 μsec

SECTION 4

PERFORMANCE ANALYSIS

In this section, we analyze the performance of several variants of RAST. The performance of both the acquisition and tracking subsystems of these variants is examined. The system realizations considered are grouped according to the type of satellite antenna which they employ; those which utilize a single beam CONUS coverage antenna and those which use a high gain 30 ft dish, maintaining CONUS coverage with a multiple beam capability. Subsidiary distinctions based upon signature structure and/or transmitted power are also considered in evaluating performance. All analyses in this section assume the use of only four satellites with RAST; this is the minimum number required for hyperbolic multilateration.

4.1 SUMMARY OF PERFORMANCE CONCLUSIONS

The performance analysis indicates that single beam realizations employing transmitters with 500 W peak power provide poor acquisition and tracking performance. With a 6 dB increase in transmitter power (2 kW), the acquisition performance becomes marginally acceptable and the tracking performance adequate. The multiple beam realizations are shown to be capable of adequate acquisition and tracking using 500 W transmitter power.

Our program of performance analysis is as follows. We begin by stating the measures which characterize the performance of both the acquisition and tracking subsystems. Evaluation of these measures requires estimates of the signal and noise energies for the aircraft-to-satellite links under consideration.

A power budget providing these values is introduced and discussed as a prelude to the analyses.

4.2 PERFORMANCE MEASURES

The remainder of Section 4 deals with the specification and performance analysis of several realizations of RAST. Therefore, it is pertinent at this point to identify the criteria by which the performance of RAST is to be judged. Performance measures for the acquisition and tracking subsystems are now defined for this purpose.

4.2.1 Acquisition

P_M, the acquisition miss probability, will be used to measure the performance of the acquisition subsystem. It is defined for the aircraft to be acquired as:

$$P_M = 1 - \text{Prob}\left\{\begin{array}{l}\text{The TOA quadruplet which is supplied}\\ \text{to the tracking subsystem corresponds}\\ \text{to the correct TOA's}^{*}\text{ of the aircraft's}\\ \text{signature at the four satellites.}\end{array}\right\} \qquad (4.1)$$

An "acquisition miss" implies that the aircraft is either not acquired or is acquired incorrectly, i.e., its track file is initialized with an incorrect position. P_M depends upon a variety of parameters; the update period, the sampling rate, signal energy, receiver noise[†] and mutual interference. An upper bound to P_M is derived in Appendix B.

---

*A "correct" TOA estimate is one that is within ± one chip duration of the true TOA.

†By receiver noise we shall mean the white Gaussian background noise at the input to a matched filter receiver. This may result from a variety of sources; thermal noise, galactic noise, RFI, etc.

4.2.2 Tracking

The rms time of arrival error due to receiver noise and mutual interference, ε, will be used to measure the performance of the tracking subsystem.

$$\varepsilon = \left\{ \begin{array}{l} \text{The rms error, due to receiver noise} \\ \text{and mutual interference, in estimating} \\ \text{the arrival time of an aircraft signa-} \\ \text{ture at a satellite.} \end{array} \right\} \qquad (4.2)$$

A lower bound to ε is derived in Appendix C.

The value of ε, measured in nsec, is approximately equivalent to the rms aircraft range error* in feet. This range error is a principal component of the overall position error of the aircraft. Further discussion of position error is found in Section 4.6.

The value of ε is determined primarily by the signal-to-receiver noise ratio, the number of in-beam interfering users and the a priori uncertainty in the signature TOA. Range estimation accuracy exhibits two contrasting modes of behavior as a function of these three parameters. When the number of interfering users is large, the accuracy is limited by the level of received interference; an increase in aircraft transmitter output power does not decrease ranging error significantly. If the number of users is small, ε is limited by the received pulse signal-to-noise ratio and the number of pulses per signature. The analysis in Section 4.5 illustrates the manner in which these factors interact to determine the range measurement accuracy possible with RAST.

*Due to receiver noise and mutual interference.

4.3 AIRCRAFT-TO-SATELLITE LINK BUDGETS

In analyzing the performance of the various RAST realizations, we shall consider the acquisition and tracking of a disadvantaged aircraft in the presence of signatures received from other aircraft. This task requires estimates of the received signal energy of signature pulses from both a disadvantaged and a typical user. In this section, power budgets are introduced which provide estimates of the signal energies and signal-to-noise ratios.

The quantities of major interest in the subsequent analyses are: the typical received signal energy per pulse (E_a), the receiver noise power density (N_o), the received signal-to-receiver noise ratio (E_a/N_o), the equivalent noise power density of the mutually interfering pulses (N_m)*, the total effective noise power density (N_{eff}, the sum of N_o and N_m), the typical effective signal-to-noise ratio (E_a/N_{eff}) and the effective signal-to-noise ratio for a disadvantaged user (E_p/N_{eff}). Each of these is computed in the aircraft-to-satellite power budget (Table 4.1) for both a single beam and a multiple beam realization. A single pulse signature is assumed. The following brief discussion of the entries should be sufficient to explain the assumptions utilized in the power budget. Many of the entries are identical to those in Table 4.2 of Vol. I,[8] and the reader may wish to review the discussion in Section 4 of that report in conjunction with the RAST power budget.

The transmitted pulse energy corresponds to a 500 W transmitter and a 50 μsec pulse length. This should be obtainable with an output tube mounted in a sheet metal cavity. It is a reasonable choice based on today's technology. The duty cycle for a 50 μsec pulse is small enough to allow adequate heat dissipation

*This is the noise power density which would result if the mutual interference had the same effect as an equivalent power in-band white noise source.

TABLE 4.1

POWER BUDGET FOR SINGLE PULSE RAST

	Single Beam		Multibeam	
Transmitted Pulse Energy		-16 dBJ		500 W, 50 μsec
Aircraft Antenna Gain		2.5 dB		average upper hemisphere
Miscellaneous Losses		-2 dB		feed, atmospheric, cable, etc.
Path Loss		-192 dB		1600 MHz, 35,000 mi
Peak Satellite Antenna Gain	24 dB		42 dB	
Thermal Distortion	0 dB		-2 dB	
Shadowing	0 dB		-1 dB	
Received Signal Energy (Typical)	-183.5 dBJ		-168.5 dBJ	
Received Noise Power Density		-201 dBW/Hz		600°K
Received Signal-to-Noise Ratio	17.5 dB		32.5 dB	
Number of Pulses Per Second		37 dB		50,000 aircraft, 1 pulse/10 sec/ aircraft
Fraction in Beam	0 dB		-7 dB	
Receiver Bandwidth		70 dB/Hz		100 nsec DPSK chips
Multiple Access Noise Power Density	-216.5 dBW/Hz		-208.5 dBW/Hz	
Effective Noise Power Density	-201 dBW/Hz		-200 dBW/Hz	
Signal-to-Noise Ratio	17.5 dB		31.5 dB	
Antenna Disadvantage (A/C)		-3.5 dB		elevation angle $\geq$ 15°
Off Boresight Loss (Satellite)	-1 dB		-3 dB	
Power Amplifier Degradation		-1 dB		
Decorrelation Loss		-1 dB		frequency offset $4:10^6$
Excess Path Loss		-1 dB		
Resultant Signal-to-Noise	10 dB		22 dB	

(see, 8, p. 23). The entry for aircraft antenna gain corresponds to the estimated average gain of an antenna maintaining uniform upper-hemispherical coverage (see, 12, p. 52). The miscellaneous feed and cable losses which occur between the transmitter and the antenna are estimated to be 2 dB. The path loss is computed at the apogee of the elliptical orbit in the constellation given in Appendix A.2 (35,000 mi).

The peak satellite antenna gain for the single beam realization corresponds to an antenna having a 10° beamwidth, the beamwidth required to maintain CONUS coverage from the specified orbits. The multiple beam antenna is the 30 ft parabolic dish (both antennas are discussed in Section 2.2.1). The 30 ft dish suffers additional losses for thermal distortion and shadowing. The entries indicated are based upon predictions for the 30 ft dish which is to be employed on the NASA ATS-F.[11]

Typical received signal energies are computed from these entries for both system realizations. When they are combined with the estimated receiver noise power density, the typical signal-to-noise ratios are found to be 17.5 and 32.5 dB, respectively, for the single and multiple beam realizations.

The acquisition analysis for RAST is carried out assuming that the effect of the mutual interference is the same as an equivalent power in-band white Gaussian noise source at the matched filter receiver. The results are given as a function of E_a/N_{eff}. N_{eff} is calculated according to the following formula:*

$$N_{eff} = N_o + \frac{fN_T PE_a}{(\alpha/\tau_c)} \tag{4.3}$$

*In this formula the signal energy is assumed to be spread over a bandwidth equal to the inverse of the chip duration.

where

N_T = Number of users

f = Fraction of aircraft in beam

τ_c = Chip duration

The computation of N_{eff} in Table 4.1 is carried out for the case in which N_T = 50,000 users, f = 0.2 (one beam covers roughly 1/5 of CONUS) and τ_c = 100 nsec. The coverage assumption corresponds to the most widely spread contours found in the maps in Appendix A. In the single beam realization, the received energy per pulse is so small that the mutual interference does not noticeably change the effective noise power density. In the multiple beam case, mutual interference raises the effective noise power 1 dB above N_o.

Thus far the received signal energy of a signature pulse from a typical aircraft has been computed using average link parameters. Additional losses are taken into account in computing the received energy, E_p, for a disadvantaged user. The aircraft antenna disadvantage is based on the desire for usable signal energy at elevations greater than 15° (relative to the aircraft). For example, this might correspond to an aircraft in a 30° bank and a satellite 45° from zenith. The indicated loss corresponds to the minimum gain in the measured pattern of a crossed-slot antenna at 75° off boresight relative to the average gain above 15° (see, 12, p. 52).

The intended aircraft may not be in position to experience the peak satellite antenna gain. In the single beam case the off boresight loss will be small due to the broad antenna beamwidth. The estimated 1 dB loss for the

earth coverage beam assumes an oversized antenna with tapered illumination. These techniques are not as appropriate for the already large multiple beam antenna and hence a 3 dB loss is taken for aircraft located at the beam edge.

The power amplifier degradation of 1 dB represents a conservative estimate relative to present day standards. Although Colby and Crocker report greater than 3 dB power variations for current transponders,[13] it may be reasonable to anticipate tnat power can be maintained to within 1 dB.

The decorrelation loss of 1 dB corresponds to a frequency offset-signal duration product of $\Delta f\tau = 0.3$. For a 50 μsec signal this implies an offset $\Delta f = 6$ KHz. This stability (four parts in 10^6) should be readily achievable for even inexpensive avionics.[14]

To account for path length differences and atmospheric absorption, a 1 dB disadvantage is assumed.

Taking all disadvantages into account, we find effective signal-to-noise ratios of 10 and 22 dB, respectively, for the single and multiple beam realizations.

4.4 ACQUISITION PERFORMANCE

The acquisition performance of RAST is now analyzed. The analysis is carried out by first computing a general upper bound to the acquisition miss probability, P_M. The bound is then evaluated and discussed for several different RAST realizations.

4.4.1 The Upper Bound to Acquisition Miss Probability

The derivation of the upper bound to P_M assumes that the mutual interference has the same effect as an equivalent power in-band white Gaussian noise source. The bound is derived in Appendix B and is given by

$$P_M \leq 1 - \max_{p_f} \left\{ Q\left(\frac{2E_p}{N_{eff}} , \sqrt{-2 \ln p_f} \right) \right\}^P (1 - p_f)^{\frac{6\delta+\alpha}{\tau_c}} \quad (4.4)$$

In (4.4), p_f is the false alarm probability per matched filter sample and δ is the maximum time delay between receptions of the same signature retransmitted from two different satellites. $Q(\cdot,\cdot)$ denotes the Marcum "Q" function.

This upper bound is plotted as a function of E_p/N_{eff} in Figs. 4.1a and 4.1b. Figure 4.1a indicates the variation over the range from 10 dB to 20 dB assuming a single pulse signature. Figure 4.1b illustrates an enlargement of the variation over the smaller range 16 dB to 19 dB and in addition includes the results for three pulse signatures. The curves were computed assuming α = 10 sec and δ = 24 msec. It is worthwhile to note the following points concerning this bound to P_M.

1) Sensitivity

The curves indicate a threshold behavior and an extreme sensitivity to changes in E_p/N_{eff} for values above threshold. In the given curves, the threshold appears to be about E_p/N_{eff} = 16 dB. As E_p/N_{eff} is increased from 15 dB to 20 dB, the upper bound to P_M varies from approximately 10^{-1} to 10^{-8}. It is expected that the actual acquisition miss probability exhibits similar behavior.

This sensitivity in performance is not a desirable characteristic. A 3 dB error in estimating E_p/N_{eff} (i.e., 16 dB vs 19 dB) would not be inconceivable since the power budget entries are, at best, estimates. Such sensitivities must be well buffered by the provision of sufficient margin in the power budget.

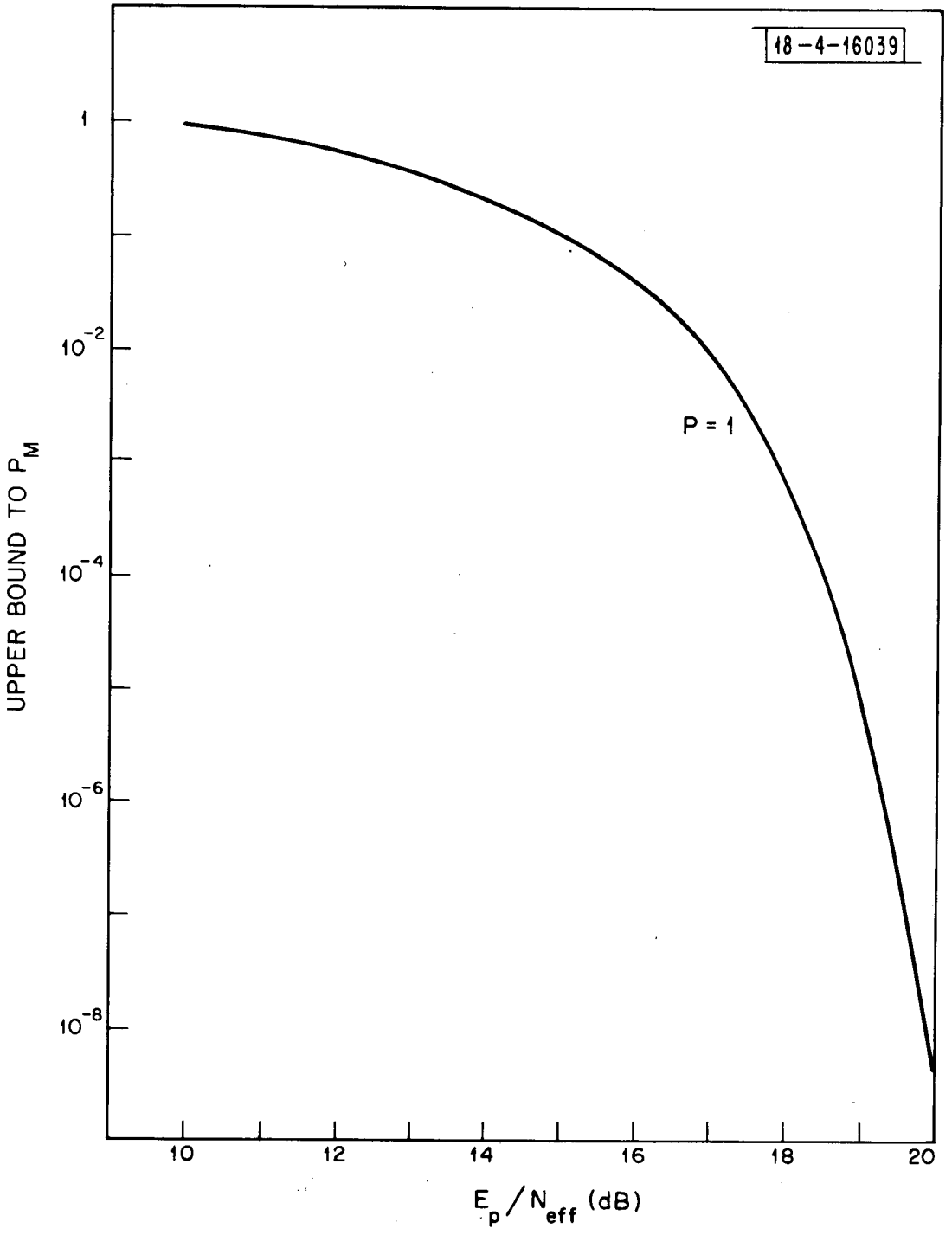

Fig. 4.1a. An upper bound to P_M vs E_p/N_{eff}.

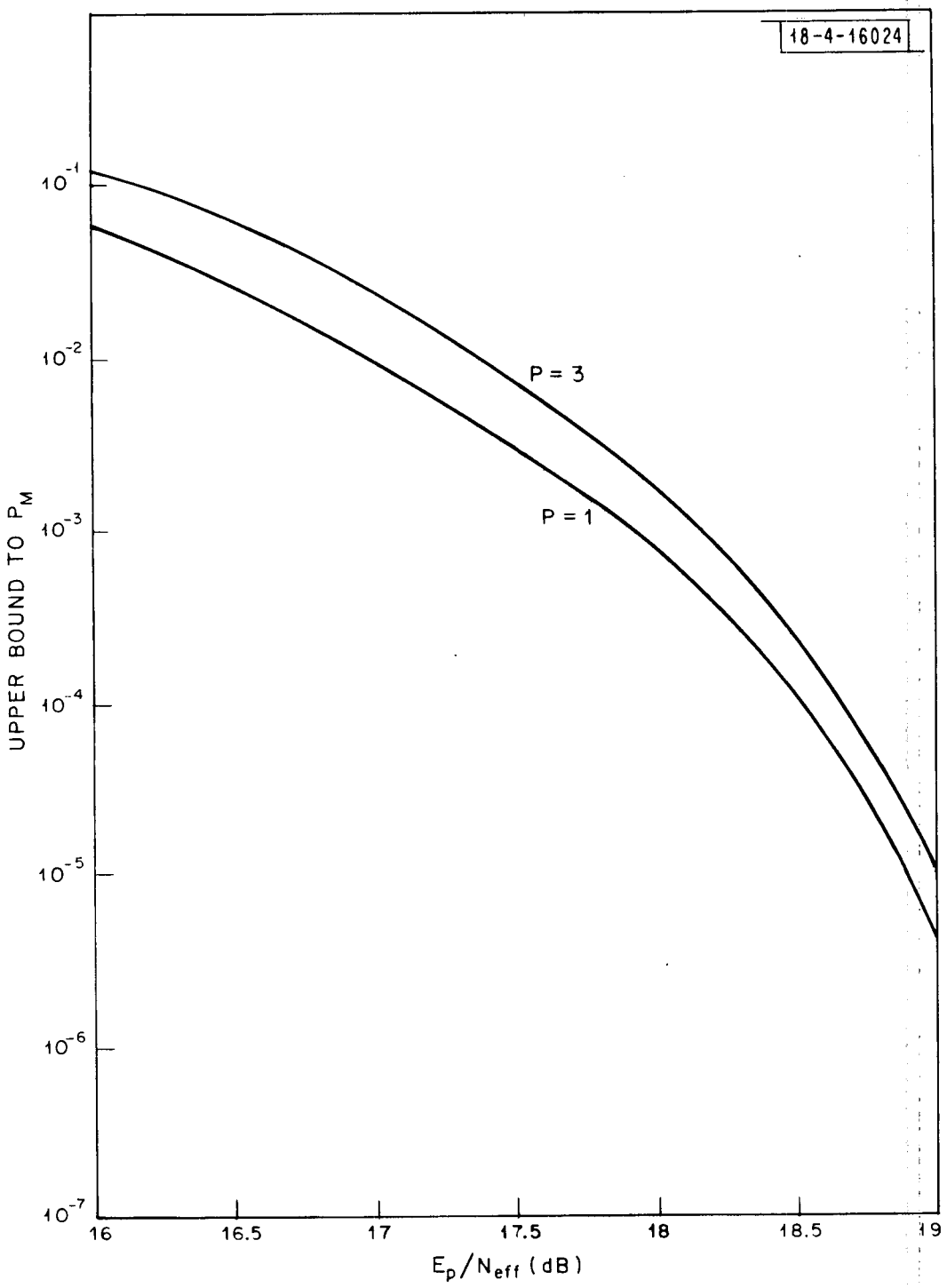

Fig. 4.1b. An upper bound to P_M vs E_p/N_{eff}: expanded scale.

2) Gaussian Advantage

Studies have been performed which compare the receiver operating characteristics (ROC's) obtained for various analyses of signal in interference-plus-noise environments. For example, Goldfein[15] has simulated a candidate system employing RAST and finds that the sample ROC's predict acquisition performance which is degraded relative to that obtained under the "equivalent in-band Gaussian noise" model for interference. These findings appear to hold over a wide range of interference environments and are supported by analyses due to Schneider, et. al.[16] The extent of the discrepancy may be as much as 6 dB in signal-to-noise ratio. Figure 4.2 exhibits an example of Goldfein's results. The ROC of the matched filter-envelope detector operating in the mixed mutual interference-white Gaussian noise environment with E_p/N_o = 22 dB and E_p/N_{eff} = 20 dB is very close to the ROC of the receiver operating in the pure white Gaussian noise environment with E_p/N_{eff} = 16 dB. These observations should be borne in mind in interpreting Fig. 4.1; the values of acquisition miss probability given there might be regarded as optimistic.

3) Increasing E_p/N_{eff}

Acquisition performance improves with increasing E_p/N_{eff}. There are several different ways to effect an increase in E_p/N_{eff}. One of these is to employ greater aircraft transmitter power. However, the benefit of this is limited by the proportionality of the signal power and the mutual interference noise power density. Above a certain power level, E_p/N_{eff} ceases to be a function of transmitter power. In addition, the burden of this improvement must be borne solely by the participating aircraft.

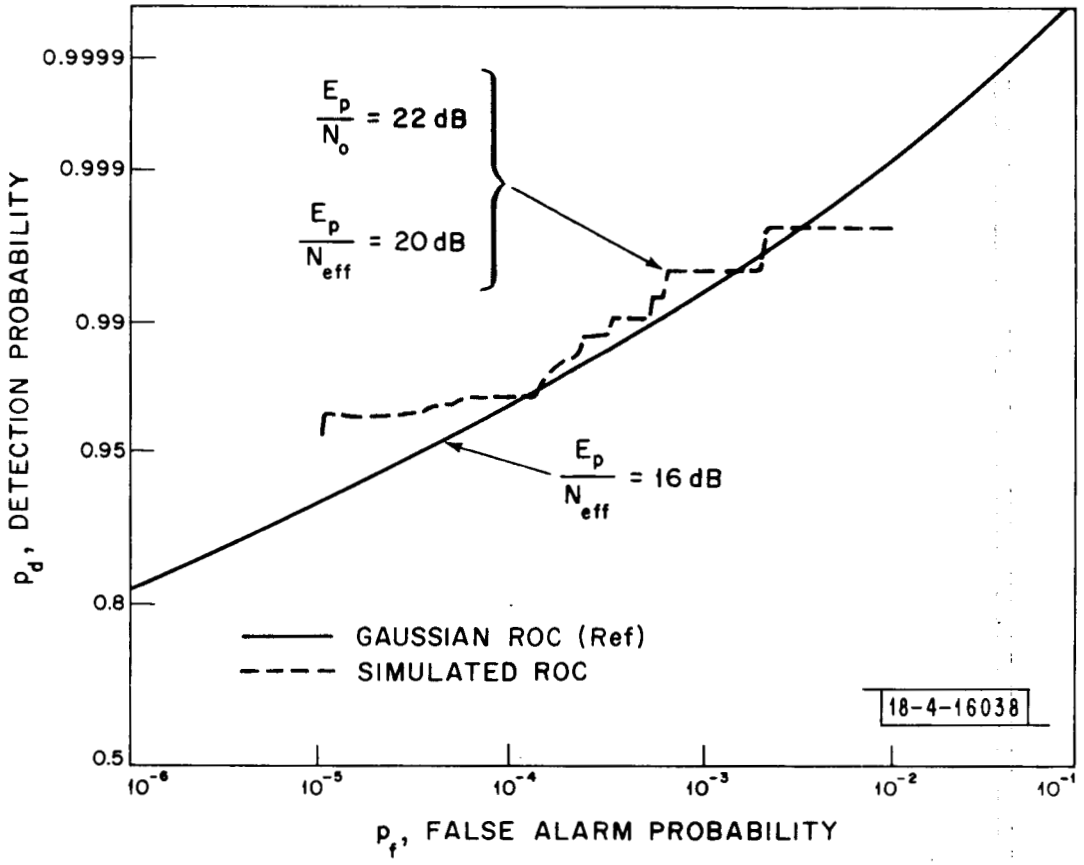

Fig. 4.2. ROC for simulated interference-plus-Gaussian noise environment.

Use of a larger (higher gain) satellite antenna enhances the signals relative to receiver noise and thus increases E_p/N_{eff}. Equally important, the smaller beamwidth of this antenna decreases the effective number of interfering users, and thereby decreases N_{eff}. In this case, the cost of the two-way improvement is distributed over the user population.

4.4.2 Acquisition Performance for Single Beam Realizations

We now examine P_M for single beam realizations using the power budget provided in Table 4.1. For a single pulse signature, the power budget estimates E_p/N_{eff} at 10 dB, assuming a 500 W transmitter power and 5000 aircraft transmitting per second. With a 10 sec update period this would imply service to 50,000 aircraft, certainly enough to encompass en route surveillance service during the 1990's. With multiple pulse signatures E_p/N_{eff} will be slightly less than 10 dB.

From Fig. 4.1 we see that the upper bound to P_M is very close to 1. The predicted performance will be even less desirable when one takes into account an allowance for margin and the Gaussian advantage. If three pulse signatures are used instead of single pulse signatures, the performance deteriorates further.

For the parameter values in this example, the performance is not interference limited. Thus, there is the possibility that P_M will decrease significantly with increasing transmitter power. Suppose the power is increased to 2 kW. For both types of signatures E_p/N_{eff} will be increased to about 16 dB. From Fig. 4.1 it is noted that at $E_p/N_{eff} = 16$ dB, the upper bound to P_M is approximately 0.1 for $P = 1$ and $P = 3$. On the surface this represents acceptable

system performance. It implies that on the average 10% of the aircraft to be acquired during one update will be missed. However, most of these aircraft will probably be acquired in the next update period or when any erroneous tracks generated by the misses fail the reliability test.

Again, one should be wary of the adequacy of this system. No margin has been allotted either for the Gaussian advantage or for any optimistic entries in the power budget. The E_p/N_{eff} of 16 dB is near the threshold point. This is hardly a desirable operating point for a system. In addition, this marginal performance requires a considerable increase in avionics cost (see, 8, Fig. 3.5).

4.4.3 Acquisition Performance with Multiple Beam Realizations

For the multiple beam realizations, the power budget provided in Table 4.1 indicates that E_p/N_{eff} is about 22 dB for both single and three pulse signatures. The 5000 aircraft which transmit per second are assumed to be divided equally among five satellite antenna beams. The nominal 500 W transmitter power is assumed.

From Fig. 4.1, we see that when E_p/N_{eff} = 22 dB, P_M is at most 10^{-8} for either the single pulse signature or the three pulse signature. This is exceptional performance. On the average, at most one out of 10^8 acquisitions will be missed. Even if the Gaussian advantage and/or the sensitivity are taken into account, the performance still remains more than acceptable. For example, if we take off 6 dB to account for these effects, E_p/N_{eff} will be at least 16 dB, implying an upper bound to P_M of 10^{-1}. As noted previously, this could easily be acceptable performance. We can conclude that the multiple beam realization would operate near threshold only in the worst case circumstance.

4.5 TRACKING PERFORMANCE

The analysis of the tracking performance of RAST is described in this section. The features of the signature and channel models are more important to this analysis than to the acquisition analysis and are consequently reviewed prior to presentation of the performance predictions.

4.5.1 Signature and Channel Model Features

Several properties of the aircraft signature affect the performance of the tracking subsystem. Among these, the number of pulses is of special interest since it influences the performance in several different ways. It is helpful to understand how various advantages and disadvantages accrue from the selection of the number of pulses per signature.

Multiple pulse signatures are attractive since they provide several pulse TOA estimates which can be effectively averaged to obtain a signature TOA estimate. This averaging results in a reduction of the rms signature TOA error by a factor of $\sqrt{P}$ relative to the rms pulse TOA error. On the other hand, the repeated use of a particular elementary pulse in more than one signature can be a disadvantage. During the tracking of an aircraft, the receiver may detect spurious pulses which are identical to those in the aircraft signature, but which actually have been transmitted by some other aircraft. The TOA measurements resulting from reception of these spurious pulses can be highly erroneous.

Single pulse signatures do not have the advantage of improved accuracy due to pulse TOA averaging. On the other hand, they do not give rise to any confusion in associating pulses with parent signatures. The performance trade-off between multiple pulse and single pulse signatures is far from obvious,

and for that reason tracking performance is investigated for examples of both signature types.

In analyzing the TOA errors for RAST, we use a model which differs considerably from those used previously for this task. The most common treatment of mutual interference has been to assume that its effect at the receiver is the same as an equivalent power in-band white Gaussian noise source. In the model employed here for tracking analysis the interference is represented by a filtered Poisson process. In Section 4.4, we have noted that these two models predict noticeably different acquisition performance. In using the Poisson model, we have attempted to more closely approximate the physical signal processes present at the receiver and have obtained the following lower bound to the mean-squared time of arrival error, ε^2 (see Appendix C, Eqs. (C-39) and (C-40)):

$$\varepsilon^2 \geq \frac{1}{P}\left[e^{-\frac{fN_TPT_o}{N}}\,\overline{e^2} + \left(1 - e^{-\frac{fN_TPT_o}{N}}\right)\frac{T_o^2}{3}\right] \qquad (4.5)$$

All quantities in (4.5) have all been defined earlier in this report (Sections 2.2 and 4.3) with the exception of $\overline{e^2}$; $\overline{e^2}$ is the lower bound to the single pulse TOA error (C-33). The coefficient, $\exp(-fN_TPT_o/N)$, is the probability that no spurious pulse occurs. In the second term, $T_o^2/3$ bounds the worst case TOA error due to a spurious pulse arrival. It is assumed that the spurious pulse has greater energy then the pulse from the disadvantaged user and consequently the TOA estimate is essentially the spurious pulse TOA. This TOA is uniformly distributed over the uncertainty interval. The effect of pulse averaging is evident in the leading coefficient. Equation (4.5) is used for all the TOA error calculations in the remainder of this section.

4.5.2 Tracking Performance of Single Beam Realizations

The tracking performance of the system realizations which employ single beam CONUS coverage satellite antennas is now examined. First, we consider the performance when a nominal 500 W transmitter is employed. Table 4.1 provides the power budget for this realization and shows that E_p/N_o = 10 dB. This is the same as the value of E_p/N_{eff} and indicates that the interference is small relative to the receiver noise. Suppose we ignore for the present all effects due to mutual interference. The TOA error analysis for the resulting known signal-in-noise problem can be found in Orr and Yates[17]; that analysis provides the following lower bound to ε for a general P pulse RAST signature:

$$\varepsilon \geq \frac{T_o}{2\sqrt{P}} \sqrt{Q\left(\sqrt{\frac{E_p}{N_o}}\right)} \qquad (4.6)$$

$Q(\cdot)$ is the Gaussian probability distribution defined in (C-6).

Evaluating (4.6) for a representative uncertainty window of 5 μsec (see Table 3.1) yields the following lower bounds to ε:

$$\text{(single pulse):} \quad \varepsilon > 80 \text{ nsec} \qquad (4.7)$$

$$\text{(three pulse):} \quad \varepsilon > 46 \text{ nsec} \qquad (4.8)$$

These correspond to undiluted rms range errors of at least 80 ft and 46 ft, respectively. Whether errors of this magnitude are acceptable for a surveillance system depends upon several additional factors, such as constellation GDOP,

detailed system requirements, etc. A more extensive analysis using the results of Appendix C indicates that these error bounds become even larger for interference rates in excess of 10^4 users/sec.

Suppose that the transmitter power of the single beam realizations is increased by 6 dB from the nominal 500 W to 2 kW. Lower bounds to ε have been computed in this situation for both single pulse and three pulse RAST signatures* (C-33, C-40). They are plotted in Figs. 4.3 and 4.4 as functions of the number of aircraft serviced/sec.† Both figures contain three curves corresponding to uncertainty window widths of 20, 5 and 1 μsec. The general characteristics of these curves are of interest.

Figure 4.3 (single pulse signature) indicates a strong threshold behavior in TOA error as a function of the number of users per second. For each of the given uncertainty windows the threshold is at about 10^4 users/sec. The fact that each of the curves approaches the same asymptote at low service rates demonstrates that the signal-to-noise ratio E_p/N_o is in each case large enough for the TOA error to be approximately that predicted by the Cramer-Rao bound.

The threshold is far more gradual for the three pulse signature (Fig. 4.4); over the range of service rates indicated, thresholding is evident only on the T_o = 1 μsec curve and it occurs at a lower service rate. In fact, a comparison of the 1 μsec window curves in the two figures illustrates that the performance trade-off between a single and a multiple pulse signature is a rather complex issue which cannot be fully discussed here.

---

*For the case of three pulse RAST signatures, the bounds were derived assuming an elementary pulse set of 100 members, so that it is possible to construct $10^6 = (10^2)^3$ signatures without using the interpulse spacing for encoding.

†These curves have been computed assuming that the chips in the DPSK signal are trapezoidal in shape with a chip duration, τ_c, equal to 100 nsec and a rise time τ_r, equal to 10 nsec.

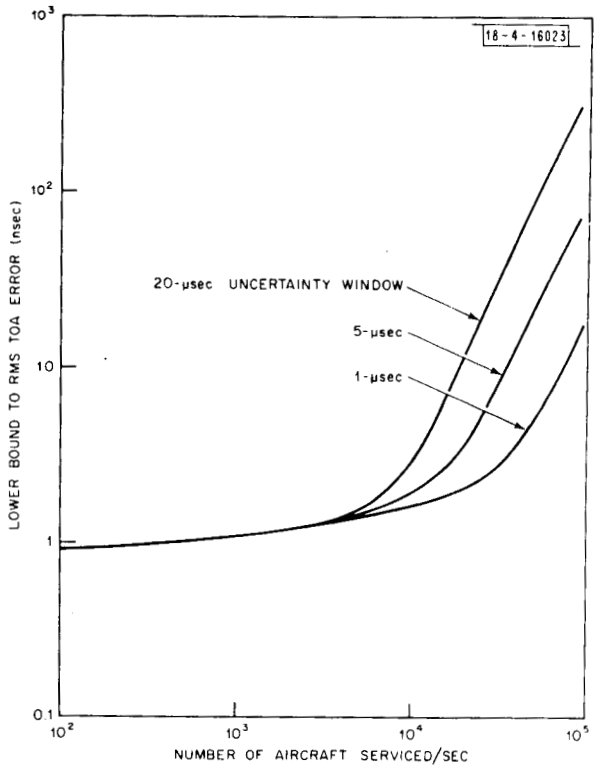

Fig. 4.3. Lower bound to rms TOA error vs number of aircraft serviced/sec for single beam, single pulse RAST. Transmitter power = 2 kW.

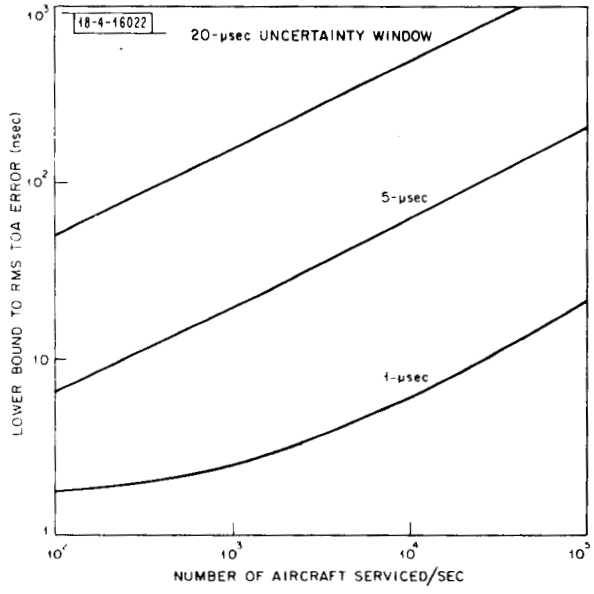

Fig. 4.4. Lower bound to rms TOA error vs number of aircraft serviced/sec for single beam, three pulse RAST. Transmitter power = 2 kW.

At low service rates, the effect of pulse averaging is evident. As the number of users increase, ambiguities due to spurious pulse receptions drive the multiple pulse TOA error up, while the single pulse error remains constant. When the number of users per second exceeds 10^5, the single pulse thresholding takes over and the single pulse case once again has the larger error. If the curves were extended to even larger populations, they would show the error saturating at a value proportion to $T_0/\sqrt{P}$. In this limit the pulse averaging effect is again seen.

We now use these curves to determine specific error estimates for the system realizations. Assume that 5000 aircraft are being serviced per second (the nominal value assumed in Table 4.1), and that the uncertainty window width is 5 μsec. Figure 4.3 indicates that with single pulse signatures the lower bound to ε for this representative case is approximately 2.5 nsec. Figure 4.4 indicates that with three pulse signatures the lower bound to ε is approximately 20 nsec. These correspond to undiluted rms range errors of 2.5 and 20 ft, respectively. These are certainly acceptable for tracking performance. However, it must be emphasized that these estimates depend strongly on the 2 kW transmitter power assumption.

4.5.3 Tracking Performance of Multiple Beam Realizations

The TOA error bounds for multiple beam realizations are illustrated in Figs. 4.5 and 4.6 as functions of the number of aircraft serviced/satellite antenna beam/sec for three uncertainty window widths. Signature assumptions are identical to those in the single beam case. Transmitted power is 500 W. The curves show characteristics similar to those presented in Section 4.5.2 for the single beam realizations.

Fig. 4.5. Lower bound to rms TOA error vs number of aircraft serviced/beam/sec for multiple beam, single pulse RAST. Transmitter power = 500 W, number of beams = 5.

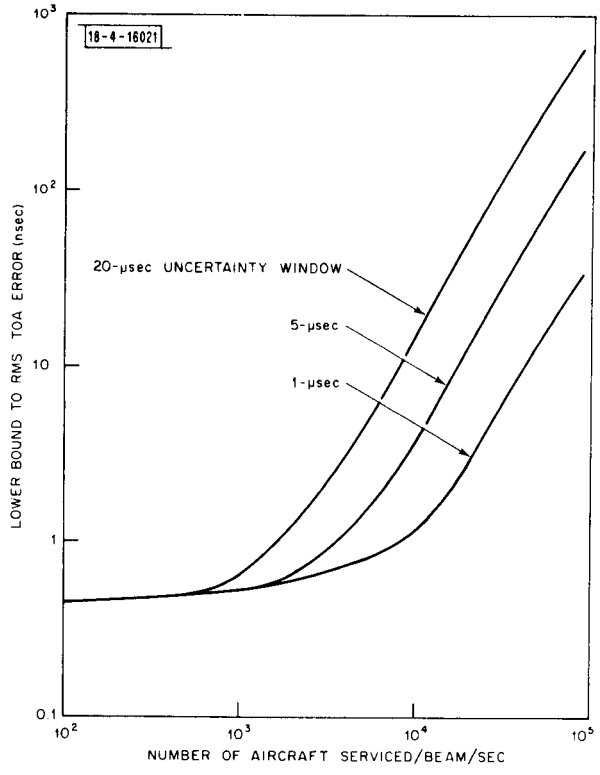

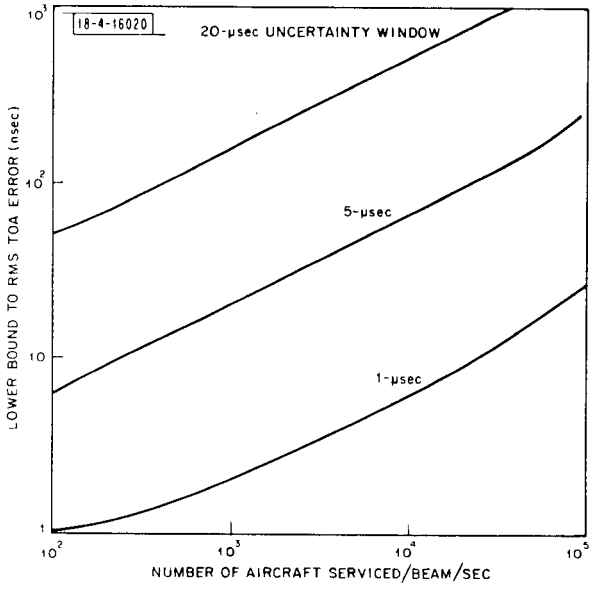

Fig. 4.6. Lower bound to rms TOA error vs number of aircraft serviced/beam/sec for multiple beam, three pulse RAST. Transmitter power = 500 W, number of beams = 5.

Let us evaluate the performance of the multiple beam realizations at the same nominal operating point used previously (5 μsec uncertainty window width, 5000 aircraft/sec). The transmitting aircraft are assumed to be uniformly spread over five satellite antenna beam coverage regions. Figure 4.5 indicates that at this service rate the lower bound to ε is approximately 1 nsec when single pulse RAST signatures are used. The corresponding error for three pulse signatures is ε = 20 nsec. These correspond to undiluted rms range errors of 1 and 20 ft, respectively. These range errors are anticipated to be adequate for tracking performance and are in fact about the same as the accuracies achieved in the high power (2 kW), single beam realizations.

4.6 POSITION MEASUREMENT ERROR IN SYSTEMS EMPLOYING RAST

We have evaluated the tracking performance of systems employing RAST by using the rms TOA (or ranging) error due to receiver noise and interference. However, this is only one component in the total rms position error. It will be worthwhile to close this section with some discussion of the overall rms position error achievable by a system employing RAST.

The rms position error is expressable as a product of two factors: the equivalent ranging error and the GDOP. The ranging error factor is the effective error in estimating the range between a satellite and an aircraft. The primary sources of ranging error are excess ionospheric delay, satellite ephemeris error and TOA estimation error. The exact values of these depend on satellite deployment, satellite tracking and calibration station implementation, satellite orbital parameters, the central processing facility, link characteristics (multipath, signal format, signal level, receiver noise, antenna gain, etc.), clock accuracy, etc.

With RAST, ionospheric errors can be kept within bound by using a network of calibration stations employed to estimate the excess ionospheric time delay for use in correction of position determination data. For elevation angles exceeding 30°, the worst case* excess ionospheric ranging error is estimated to be at most 20 ft.[18] The satellite position is to be determined using satellite equations of motion (for an assumed geopotential model) to smooth satellite position data obtained from a network of tracking stations. The resulting effect on the ranging error term should be no more than 20 ft.[5] We have demonstrated several system variants for which the TOA estimation error can be kept below 20 nsec at service rates of interest. Thus, it is reasonable to expect that the overall rms ranging error due to noise, mutual interference, clock instability. nonoptimum processors, etc., should not be more than 40 ft.

The GDOP is determined by the number and disposition of the satellites within view. Constellations which exhibit GDOP's ranging from 3 to 6 over CONUS are presented in Lee and Wade.[10] The constellation candidate presented in Appendix A and used for the coverage analysis is one of those. If that constellation is employed, the resulting rms position measurement error is estimated to be approximately 120 ft. This resulting error value should be taken only as a guide to the position error achievable with RAST and not as a firm system parameter. Determination of a refined estimate of the accuracy requires additional ionospheric data, a detailed system design for the tracking network and a more detailed analysis of the errors in the TOA estimation implementation.

*During periods of high solar flux, near equinox and in early afternoon.

SECTION 5

CRITICAL SYSTEM ISSUES

Thus far, the assessment of RAST has concentrated upon determining the ability of these techniques to provide ATC surveillance service. The objective of this section is to examine two ancillary issues which are important to understanding broader-based aspects of RAST. These are; the vulnerability of a system employing RAST to intentional jamming and the nature of the computational complexity at the system ground station. We conclude that: (1) such a system could be disabled by a few low-cost jammers, e.g., 41 dBW ERP transmitters (100 W RF power and a 3-ft antenna); (2) even using advanced techniques, the real-time signal processing and digital computation demands for RAST surveillance require many tens of high speed parallel processors of various sorts.

5.1 VULNERABILITY TO JAMMING

Because surveillance systems employing RAST rely upon an uplink for ranging, such systems are potentially susceptible to interference from terrestrial jammers. We evaluate the jamming threat by computing the minimum requirements which a terrestrial jammer must meet in order to disable a multiple beam realization of RAST, that is, one which utilizes a 30 ft dish as a satellite antenna and maintains CONUS coverage with a multiple beam capability.

A single beam channel will be considered disabled if the rms ranging error on that channel is driven up to or beyond 100 nsec. For the multiple beam configuration represented by the power budget in Table 4.1, nominal parameters for the disadvantaged user are E_p/N_{eff} = 22 dB and ε = 1 nsec. The signal-to-

noise ratio at which the ranging error lower bound equals 100 nsec is a function of the width of the a priori uncertainty interval. We will assume the nominal value T_o = 5 μsec. The equation which yields the E_p/N_{eff} value required to drive ε to 100 nsec ($N_{eff} \approx N_o$) is approximated by:

$$\frac{5 \times 10^{-6}}{\sqrt{8}} \sqrt{Q(\sqrt{\frac{E}{N_o}})}\text{sec} = 10^{-7}\text{sec} \qquad (5.1)$$

The solution of (5.1) is E_p/N_{eff} = 11 dB. We will assume that the jammer uses the elementary strategy of transmitting Gaussian noise which has a flat spectrum spread over a 20 MHz band encompassing the signal spectrum (recall that the chip duration is 100 nsec). The jammer power required must be sufficient to decrease E_p/N_{eff} by 11 dB. Since thermal noise completely dominates the multiple access noise, we can use N_o = -201 dBW/Hz (Table 4.1) to find that the jammer noise power density (J) must be J = -190 dBW/Hz. The jammer power budget in Table 5.1 shows that this corresponds to an ERP of 41 dBW. This ERP can be achieved by, for example, a 100 W source driving a 3 ft (15° beamwidth) dish.

About 5 such "toaster powered" jammers located at the intersections of 3 dB contours of the beam patterns would suffice to disable all 10 uplink channels. The use of a waveform more sophisticated than the assumed broad band noise could decrease the jammer power requirement.

5.2 PROCESSING AT THE GROUND STATION

The use of satellites as a relay in a surveillance link between aircraft over CONUS and ground-based installations has a concomitant requirement for centralized data processing. At the ground facility of a system employing RAST

TABLE 5.1

GROUND-TO-SATELLITE JAMMING POWER BUDGET

Jammer ERP	41 dBW
Path Loss	-192 dB
Peak Satellite Antenna Gain	42 dB
Off Boresight Loss	-3 dB
Antenna Shadowing	-1 dB
Thermal Distortion	-2 dB
Miscellaneous Losses	-2 dB
Bandwidth	-73 dB-Hz
Jammer Noise Power Density(J)	-190 dBW/Hz

where the relayed transmissions are received, at least the following operations must be performed for each aircraft:

1. Detect each signature pulse.
2. Estimate each pulse TOA for all satellites in view.
3. Associate received pulses with parent signature.
4. Precorrect TOA's for propagation delays.
5. Estimate aircraft position from TOA's.
6. Filter position estimates with past position data.
7. Determine disposition of the data and route appropriately.

In addition to the above, there are a number of routine functions which must be continually performed (estimation of excess propagation delay map, satellite position tracking, system fault detection, etc.).

A detailed assessment of the total processing requirements is beyond the scope of this report. Preliminary estimates of the complexity of some of these tasks can, however, be made for the purpose of roughly sizing the ground station requirements. The specific topics investigated in this section are; the implementation of the matched filters used to detect and measure the TOA's of the received pulses, and the digital computation required to perform the hyperbolic multilateration.

5.2.1 Matched Filtering

The matched filtering required at the ground processor could be implemented using either analog or digital techniques. For signature pulse durations of the order of 50 μsec, an analog implementation might entail the use of a SAW* device for each matched filter. An efficient digital implementation

*Surface Acoustic Wave.

today would employ an FFT* algorithm to execute the filter convolutions. Digital architectures suitable for this task range from general purpose computers to highly specialized processors designed specifically for FFT application. A number of these implementations are surveyed in order to identify the issues critical to each of them.

SAW Devices

SAW technology offers the promise of providing inexpensive analog IF filters for high time-bandwidth produce (10^3 today, 10^4 anticipated), moderate duration (10's of μsec) waveforms. Due to the infancy of this technology, it is difficult to forecast specific costs or system integration problems, but SAW is the most attractive analog technology now being developed which is suited to this task.

In a single pulse signature system employing RAST in which up to 50,000 aircraft are serviced by a constellation having on the average 8 visible satellites, a total of 400,000 SAW filters might be required to continuously monitor all aircraft transmissions. If a three pulse signature were used, (100 elementary pulses), the requirement is decreased to less than 10^3 filters at the expense of placing greater burden upon the subsequent digital computation. The analog technique appears to be a plausible realization, at least for the multiple pulse example.

Digital FFT Techniques

FFT is a generic term for a class of efficient algorithms which perform Fourier analysis on sampled-data signals. Digital filtering can be implemented with a double FFT. Specifically, the number of operations† required to matched

*Fast Fourier Transform.

†An operation is an add-multiply combination.

filter an n-point sample is approximately $2n \log_2(2n)$. Filtering of a 500 chip signature sampled at the chip rate (the minimum possible rate) requires 10^4 operations.

Consider a system employing RAST and serving 50,000 aircraft with a 10 sec update rate. In tracking the aircraft, the ground processor must perform at least one matched filtering per pulse every 10 sec. For single pulse signatures, 5×10^8 operations are required.

Various FFT implementations are possible. For example, in present day general purpose computers, execution of an operation typically requires 20 μsec. Thus, the processing of the surveillance data for one update requires $(5 \times 10^8$ op) x(20 μsec/op) x (8 satellites) $\simeq 10^5$ sec. The implied capability is 10^4 parallel processors, which is an extraordinary number. The requirement is greater for multiple pulse signatures.

Special purpose programmable digital processors exist, e.g. the Lincoln Laboratory FDP,[19] which have an order of magnitude improvement in operation time. This advance is far from sufficient to ameliorate the real time processing problem which has been described.

More recently, a hardwired FFT signal processor of novel structure (the pipeline FFT) has been built and tested.[20,21] A pair of pipeline FFT modules can be configured to continuously filter a data stream at up to 20-30 Mb/sec, a rate sufficient for the RAST example. A few hundred of these could accommodate the acquisition and tracking needs of a three pulse signature system.

5.2.2 Position Determination Computation

Position determination using RAST is accomplished by hyperbolic multilateration. The computation requirements for this task have been studied for CAST, (see 8, Section 7.2), and the results are immediately applicable for RAST. These results indicate that a present day general purpose computer could handle the multilateration processing for 100– 200 aircraft/sec. The parallel processing capability of 25-50 such computers is required for surveillance of 50,000 aircraft at a 10 second update rate. This capability approximates that which is presently at the disposal of the combined ARTCC NAS Stage A facilities.

5.2.3 Ground Processing Conclusions

First order examination of just two of the tasks which are required at the ground station of a system employing RAST indicates substantial requirements for analog/digital signal processing and digital computation. The implications of these requirements (hundreds or thousands of parallel units of various sorts) relative to the operation and maintenance of a system employing RAST are perhaps unclear in detail, but they do convey a strong impression that the design of the computational facility is a critical technical area for RAST. A more comprehensive analysis of the computational requirements would be worthwhile.

APPENDIX A

SATELLITE ANTENNA COVERAGE ANALYSIS

A.1 COVERAGE ISSUES

If a high gain, narrow beamwidth satellite antenna is to be used with RAST, a multiple beam capability is required. This raises a variety of issues concerning (1) the number of beams to be used, (2) the disposition of the beam boresight points and (3) the variation of coverage as a function of satellite orbital position.

In this appendix we consider these coverage issues, at least in part, by performing an analysis of the coverage provided by the 30 ft L-band dish specified in Section 2.2.1. Two approaches to this task are taken. The first approach uses a simple geometric model to compute an estimate of the number of beams required for complete coverage of CONUS to within 3 dB of the peak antenna gain. The model is quite simple and thus leads to results of limited accuracy. In the second approach, we compute coverage maps which display beam footprint contours on CONUS. These contours are the locus of points at which the antenna gain pattern is 3 dB below peak. By carrying out both of these computations for a variety of satellite positions, detailed conclusions can be reached concerning the coverage issues.

A set of satellite orbital parameters is required to carry out the indicated calculations. To this end we shall first introduce a representative contellation which appears to be attractive for the surveillance aspects of RAST. All orbital data required by the coverage computations will be based upon this constellation. Coverage from a number of orbital positions is computed.

A.2 SATELLITE CONSTELLATION

The representative constellation which we shall use for our assessment of the various coverage issues is one of those determined by Lee and Wade.[12] It is a ten satellite constellation. Three satellites are in circular synchronous equatorial orbit, and the remaining seven are in a synchronous elliptical orbit. The three equatorial satellites are at longitudes of 170°, 100° and 30° W. The elliptical orbit has longitude of perigee 100° W, eccentricity 0.35, and inclination 110°. The seven satellites are spaced uniformly in time in the orbit, resulting in a period of 3:26 hours for the constellation.

Because the inclination of the elliptical orbit exceeds 90°, the ground track* of the orbit is unusual. It is a figure eight which wraps around both poles, and has its crossover point over the southern part of CONUS. This ground track is illustrated in Fig. A.1. Successive subsatellite points are indicated at hourly intervals for the day January 3, 1973. Table A.1 provides values of the various orbital parameters for the indicated subsatellite points. Each subsatellite point is north of the crossover point for about 14 hours, and south of it for the remaining ten.

Figure A.2 illustrates an azimuth-elevation plot for the elliptical orbit as observed from 40°N, 90°W. At various points in the orbit the satellite provides coverage from north, northeast, northwest, southeast, southwest and overhead. When this is coupled with the coverage from the south provided by the equatorial satellites, it is evident that this constellation provides the multiple azimuth and elevation coverage necessary for accurate position determination.[22] Each satellite is below the horizon for about five hours. Of the

*Locus of subsatellite points.

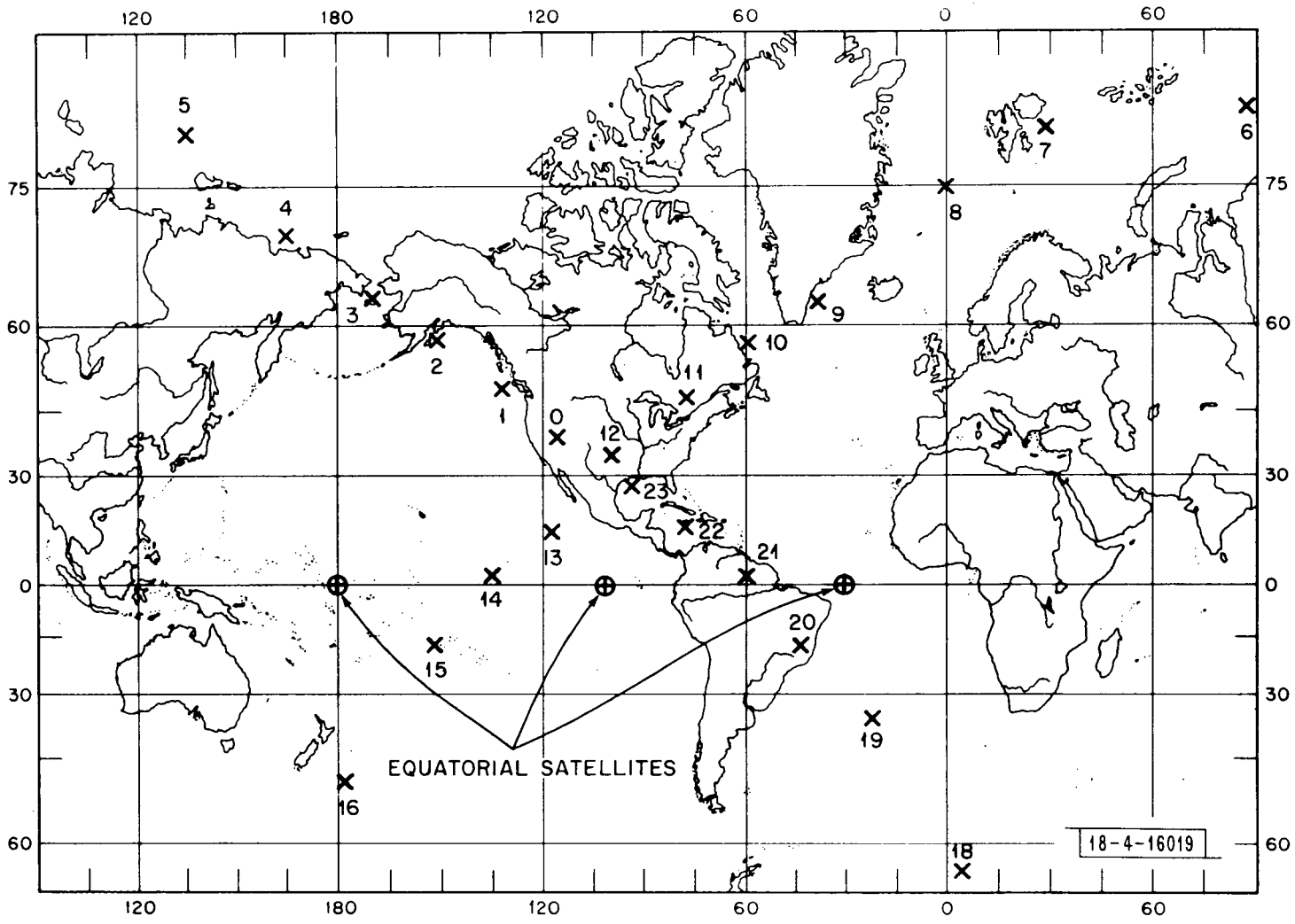

Fig. A.1. Ground track for 10 satellite constellation.

TABLE A.1

ORBITAL DATA FOR SATELLITE CONSTELLATION
(ELLIPTICAL ORBIT)

Time	N. Lat.°	W. Long.°	Elev.°	Az.°	Range (knmi)
1:00	47	133	55	298	26
2:00	55	150	43	312	27
3:00	63	170	34	325	28
4:00	70	194	27	337	29
5:00	76	226	24	349	29
6:00	80	274	24	1	29
7:00	78	331	28	12	28
8:00	73	11	36	23	27
9:00	65	38	47	32	26
10:00	56	60	61	40	24
11:00	46	80	79	47	22
12:00	34	99	79	232	20
13:00	19	117	53	237	18
14:00	2	136	24	239	17
15:00	-21	155	----------		
16:00	-49	177			
17:00	-77	232	Below the Horizon		
18:00	-64	355			
19:00	-37	23	----------		
20:00	-16	43	9	132	18
21:00	2	61	36	138	19
22:00	16	79	60	155	21
23:00	28	96	75	206	22
24:00	38	114	69	272	24

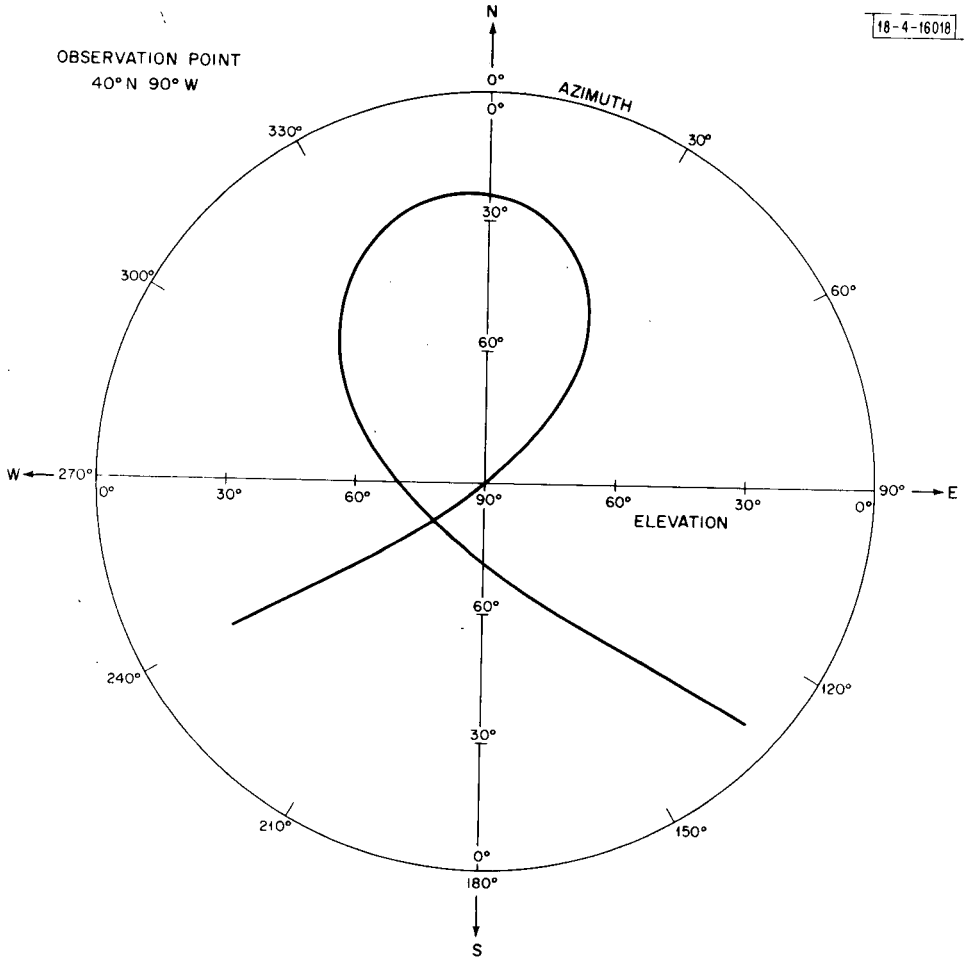

Fig. A.2. Azimuth-elevation trace for elliptical orbit of constellation.

ten satellites, eight will always be above the horizon and on the average seven will be at elevations greater than 15°.

A GDOP map for this constellation is illustrated in Fig. A.3.* At no point in CONUS does the GDOP exceed 4.7, and its average value is 2.4. The map is calculated for an aircraft in level flight; only satellites above 15° elevation are assumed to be visible. Further investigations by Lee and Wade[10] have shown that the constellation also has the desirable characteristic of relative insensitivity of position determination accuracy to aircraft orientation, satellite failure and aircraft location.

A.3 COVERAGE: GEOMETRIC APPROXIMATION

Figure A.4 illustrates the coverage geometry for one satellite antenna beam with its boresight point in CONUS. The antenna beam is assumed to be a cone of half angle $\beta/2$. Its intersection with the earth is approximately an ellipse of eccentricity

$$\varepsilon = \frac{\cos \phi}{\cos(\beta/2)} \tag{A-1}$$

and semiaxes†

$$a = \frac{R \sin\phi \sin \beta}{2 \sin(\phi+\beta/2) \sin(\phi-\beta/2)} \tag{A-2}$$

$$b = \frac{R \sin \phi \sin \beta}{2 \cos(\beta/2) \sqrt{\sin(\phi+\beta/2) \sin(\phi-\beta/2)}} \tag{A-3}$$

*Geometric Dilution Of Precision is a magnification factor which relates position measurement error to range measurement error.

†These formulas are derived from standard results for conic sections.

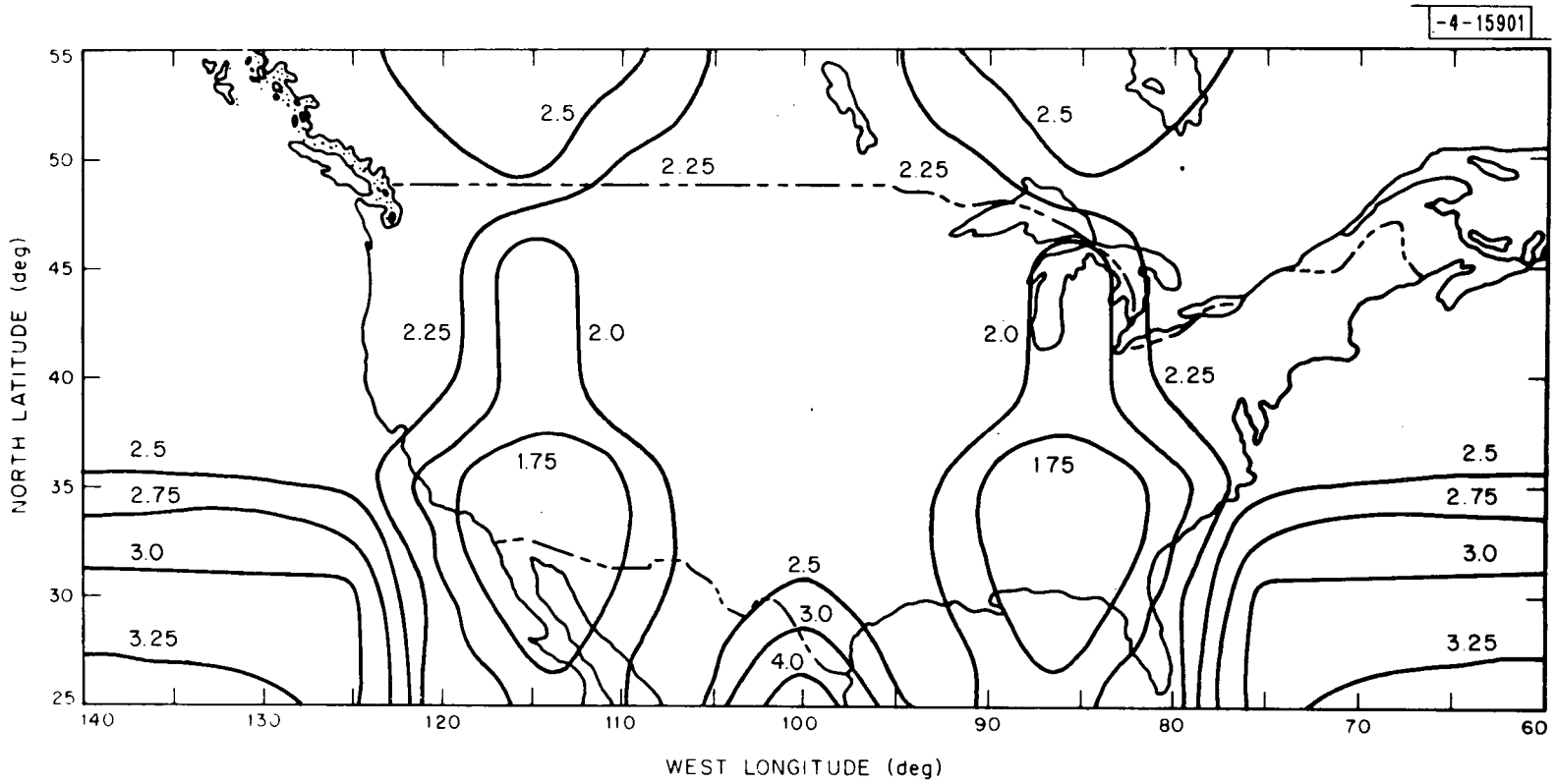

Fig. A.3. GDOP map for 10 satellite constellation.

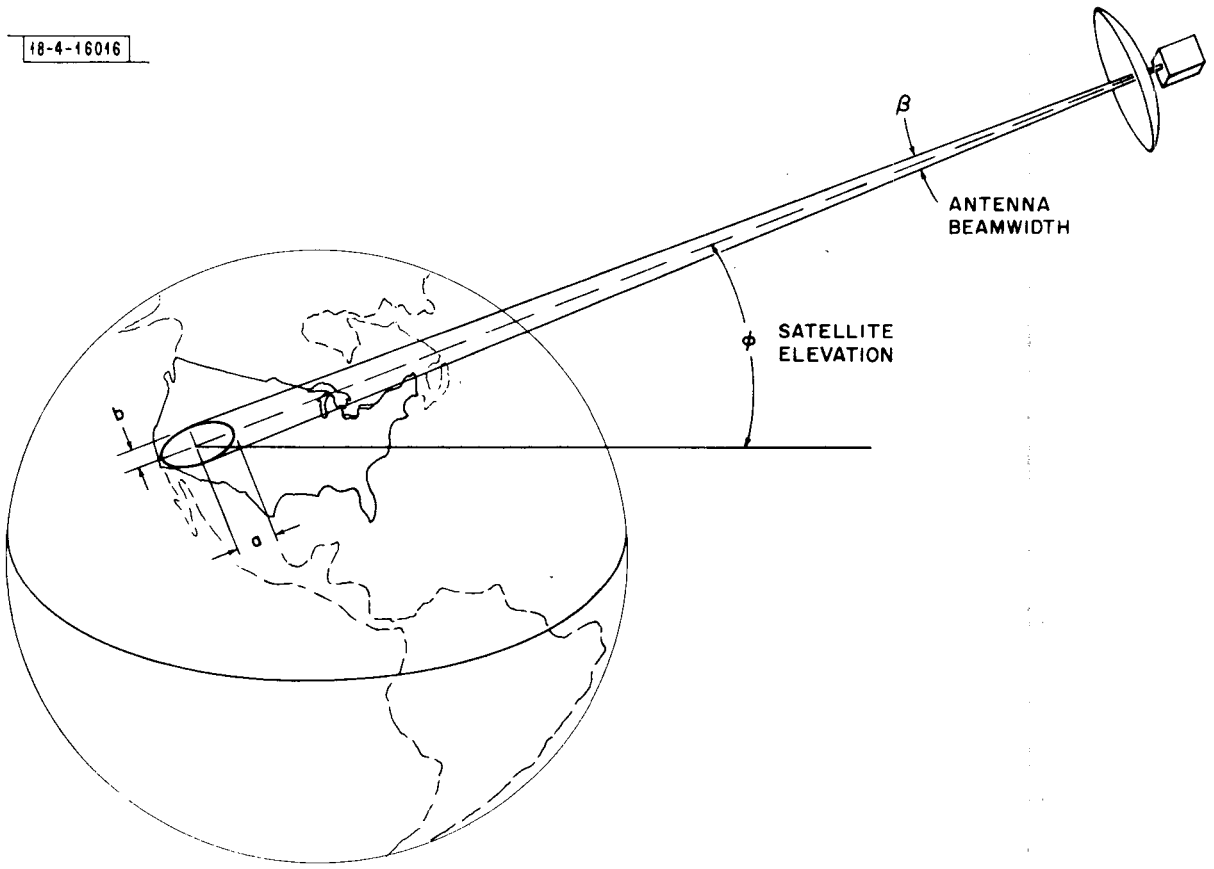

Fig. A.4. Coverage geometry from orbiting satellite.

where R is the slant range to the boresight point and ϕ is the satellite elevation as viewed from boresight. The area covered by a single beam is approximately πab (the actual coverage area will be greater because of the spherical nature of the earth's surface). An estimate of the number of beams required to cover an area A around the boresight point is

$$\text{number of beams} = \frac{A}{\pi ab} \qquad \text{(A-4)}$$

Using the above formula*, the number of beams required for CONUS coverage has been computed at hourly increments for the elliptical orbit in the constellation. The cone angle β is taken to be 1.5°, the 3 dB beamwidth of the 30 ft dish at the 1600 MHz receiving frequency. Of the 24 hourly positions, 19 have above the horizon elevation and therefore give meaningful results.

The coverage estimates obtained by this method are presented in Table A.2. The estimates range from 3 beams (for low elevation satellites) to 17 beams for satellites near the zenith. The average value is about 9 beams. Further discussion of these results is deferred to the following section, where they are compared to the predictions obtained from the coverage maps.

A.4 COVERAGE: BEAM FOOTPRINT MAPS

For the computation of the coverage maps, it was assumed that the satellite antenna uses a total of ten beams. This is roughly the average number computed by the geometric model. The boresight points (which remain stationary during satellite

*A is assumed to be the area of CONUS, 3×10^6 mi^2.

TABLE A.2

COVERAGE ESTIMATES OBTAINED FROM GEOMETRIC MODEL

Time	Number of Beams
1:00	8
2:00	6
3:00	5
4:00	4
5:00	3
6:00	3
7:00	4
8:00	5
9:00	7
10:00	10
11:00	14
12:00	17
13:00	17
14:00	9
15:00	----------
16:00	
17:00	Below the Horizon
18:00	
19:00	
20:00	----------
21:00	11
22:00	13
23:00	13
24:00	11

motion) are given in Table A.3. Five of the beam boresights are the northern part of CONUS and five are in the southern part of CONUS.

Exact beam footprints were computed using a combination of computer programs available at Lincoln Laboratory. Figures A.5 (a-t) illustrate the computed footprints for the 19 orbital points at which the satellite is above the local horizon somewhere in CONUS. Each figure also indicates the estimated number of beams required for complete CONUS coverage as computed by the geometric model (Eq. A-4).

Even a cursory examination of the beam plots shows the great variation in coverage as a function of satellite position. For example, consider Fig. A.5 l. Here the satellite is nearly overhead (elevation 79°); the 3 dB footprints for the most part do not overlap and there are large areas of CONUS which do not have 3 dB coverage. In this case, more than ten beams would be required for full CONUS coverage. In contrast, consider Fig. A.5f, for example. The satellite is near apogee and therefore appears due north at low elevation (24°). In this situation, the footprints are considerably larger than in the previous case. In fact, it appears that the five beams having northern boresights are sufficient for full coverage. In between these extremes are cases where the footprints are narrow in the East and wide in the West, or vice versa.

The coverage predictions yielded by the two methods are similar. The geometric estimates rise or fall as the beam contours exhibit lesser or greater overlap. The geometric method is most accurate for large elevation angles and in those cases the two predictions are in accord. For low elevations,

TABLE A.3

BEAM BORESIGHT POINTS

Boresight Point	Longitude (°W)	Latitude (°N)
1	124	43
2	113	43
3	102	43
4	91	42
5	75	42
6	118	35
7	107	34
8	97	32
9	87	32
10	80	31

the geometric approximation does not properly model the beam spreading over the spherical earth, and its utility is limited by the unusual shape of the contour. Thus, for example, although the coverage estimate for Fig. A.5e is three beams, the footprint plot indicates that about five are needed.

In interpreting the footprint maps it is important to take satellite range into account. In the overhead case, the satellite is nearer to CONUS than it is at apogee by a factor of about 1.5. Therefore, the actual signal energy received at the satellite from an aircraft situated on a 3 dB contour point is 3-4 dB greater in the former case than the latter. In situations where the dominant source of interference at the satellite is receiver noise, the additional gain helps to offset the gaps in 3 dB coverage which occur in the overhead case. In a more accurate comparison of received energy for various satellite positions, the 3 dB contours at apogee might be compared to the 6 dB contours for the overhead position.

It is not possible to adequately describe our assessment of the coverage issues in terms of a single number of beams which will adequately cover CONUS. We summarize this assessment of the coverage problem by stating that anywhere from 5 to 15 beams are required and that the average number is approximately 10.

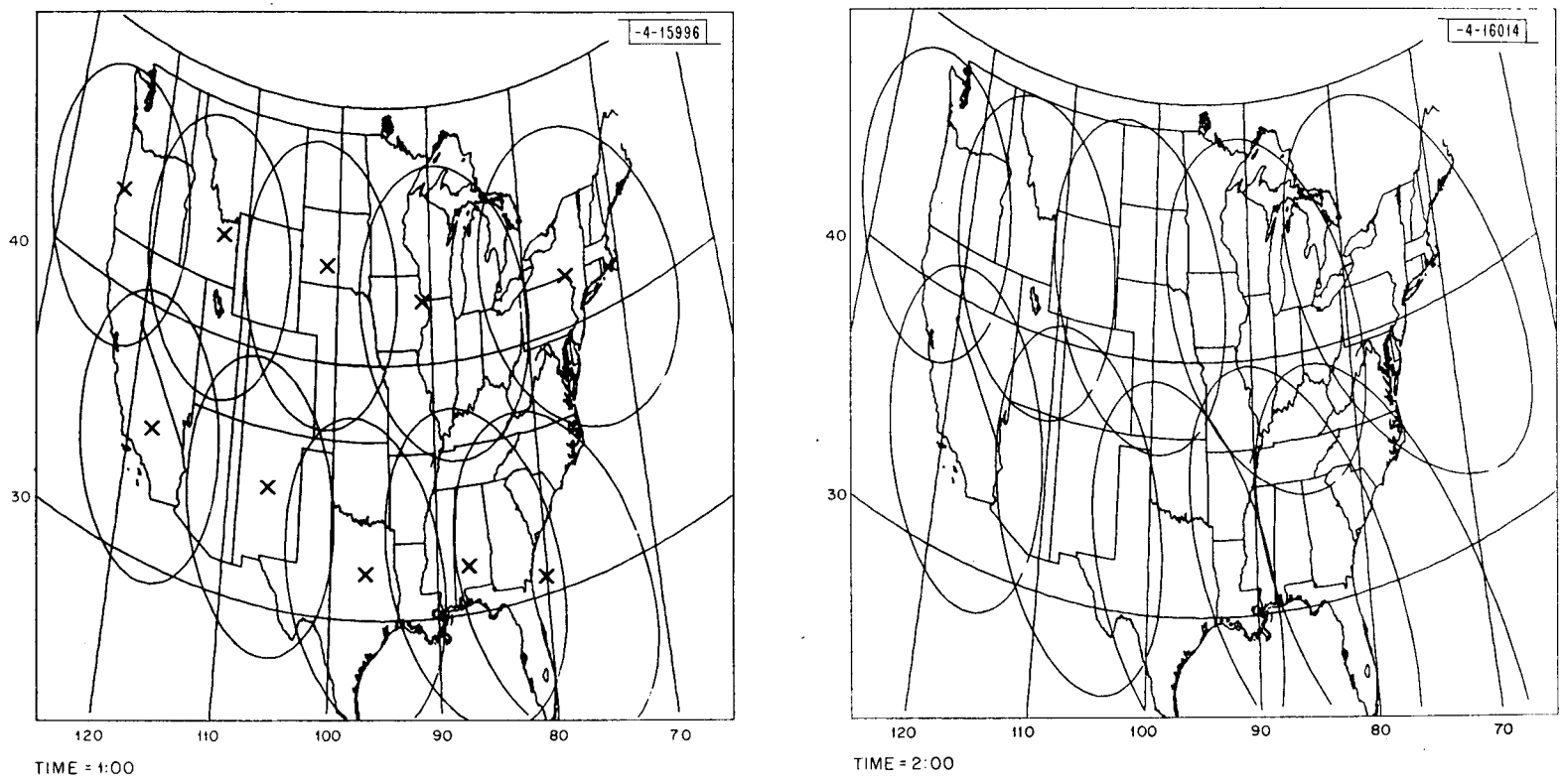

(a) (b)

Fig. A.5. Satellite antenna 3 dB coverage footprint contours at hourly intervals.

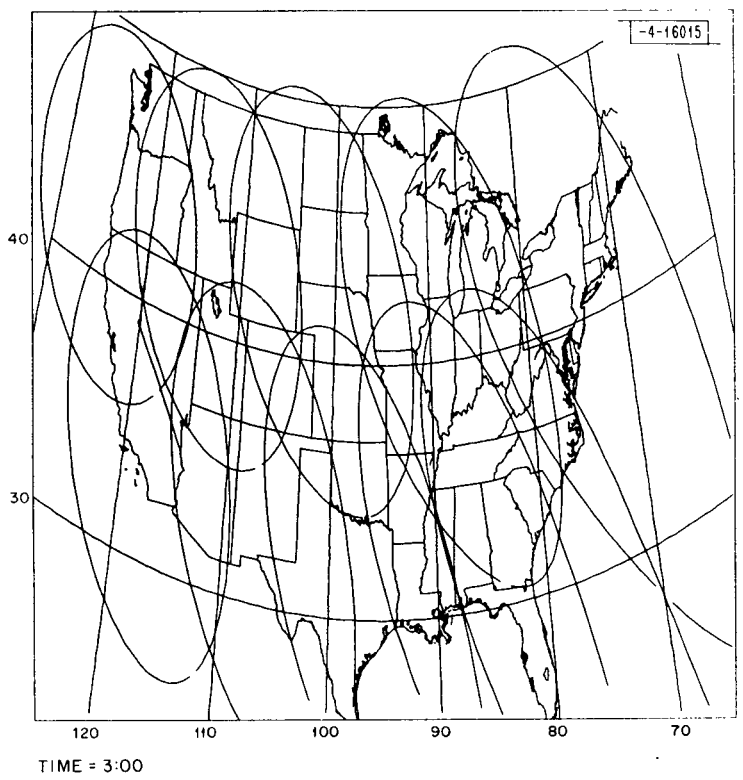

(c)

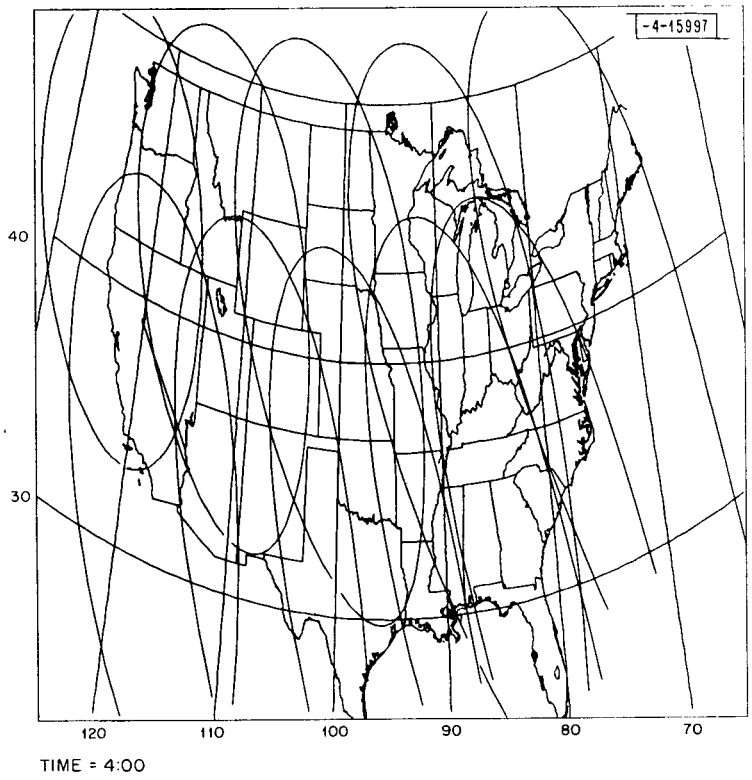

(d)

Fig. A.5. (continued).

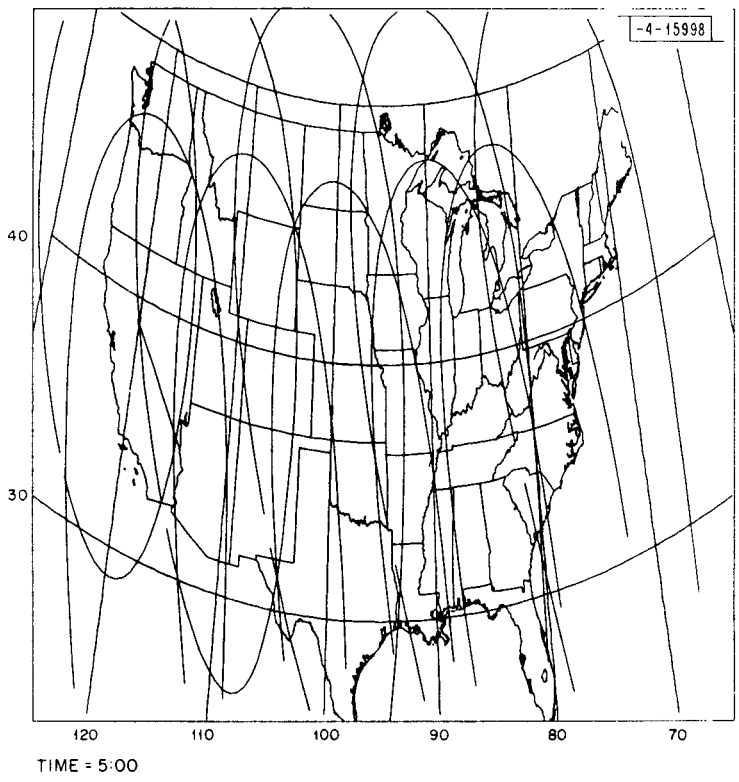

(e)

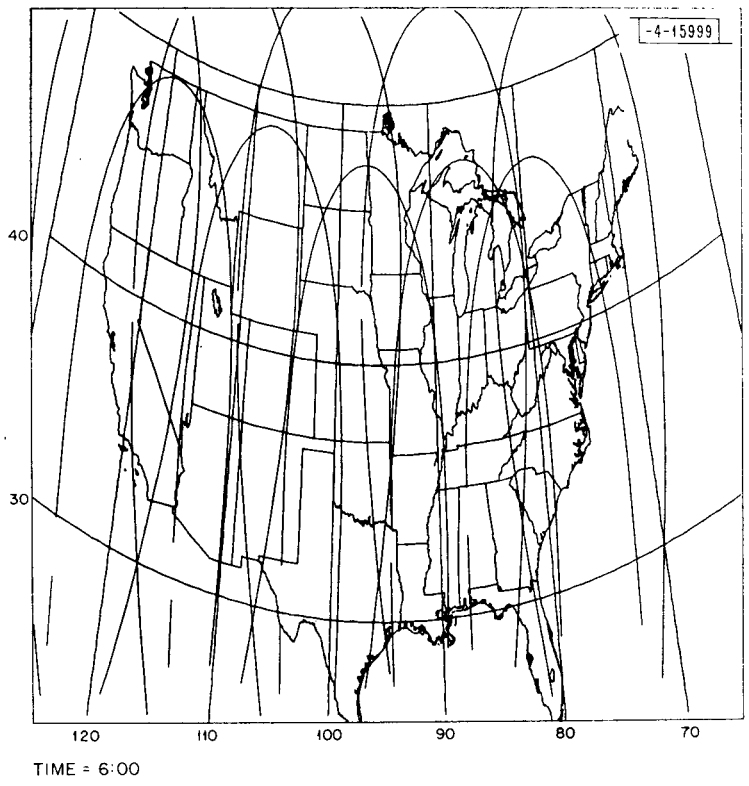

(f)

Fig. A.5. (continued).

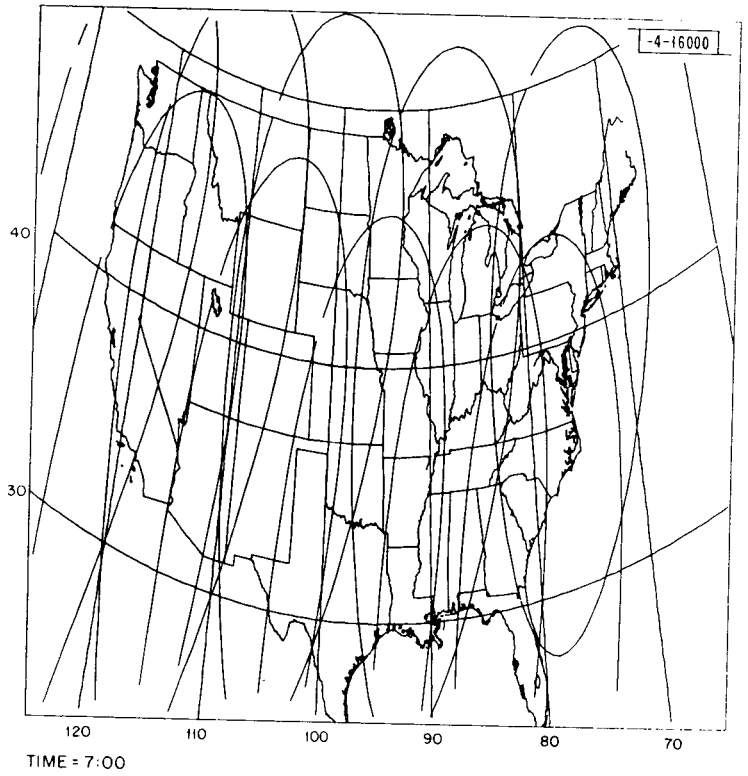

(g)

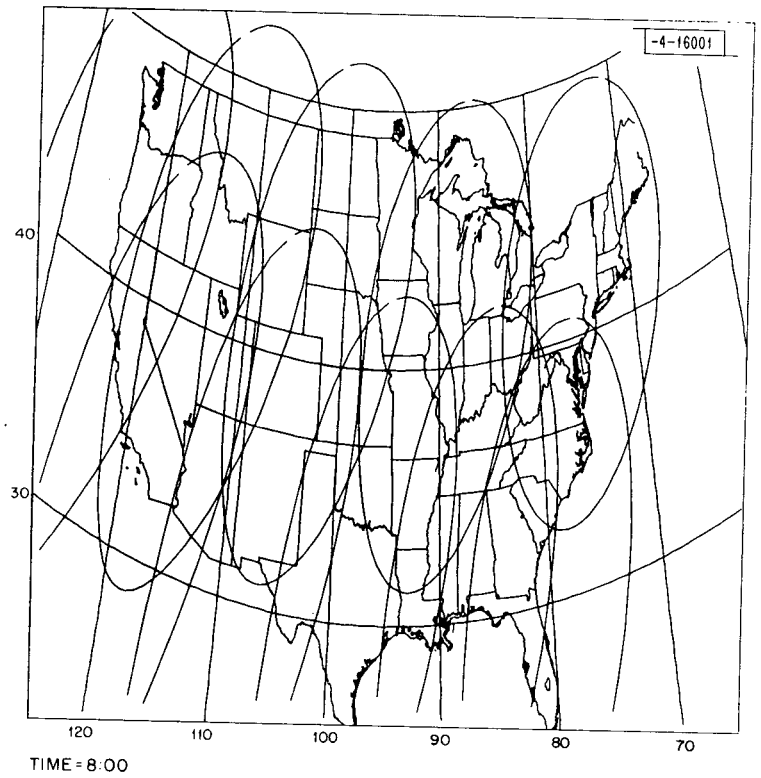

(h)

Fig. A.5. (continued).

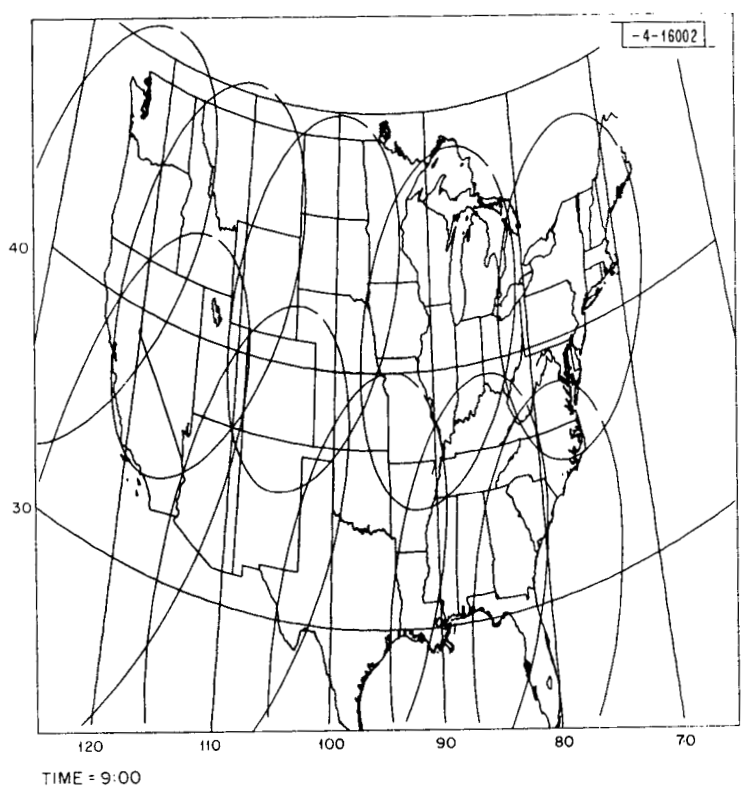

(i)

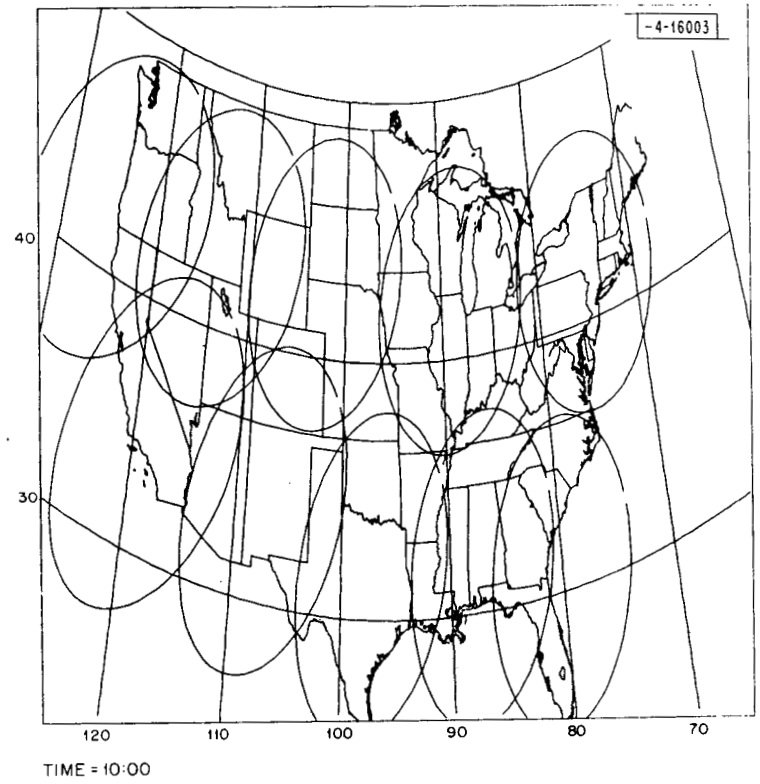

(j)

Fig. A.5. (continued).

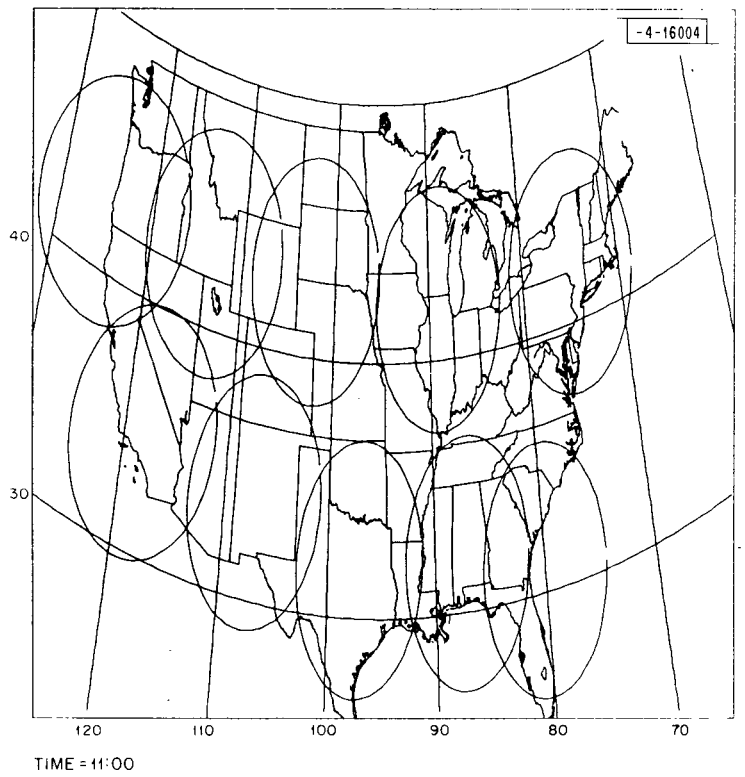

(k)

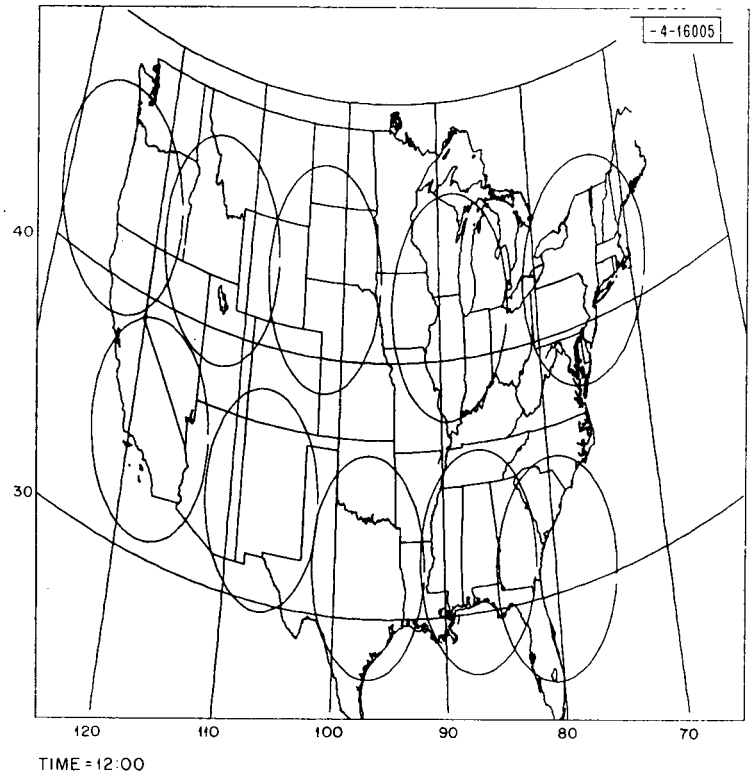

(l)

Fig. A.5. (continued).

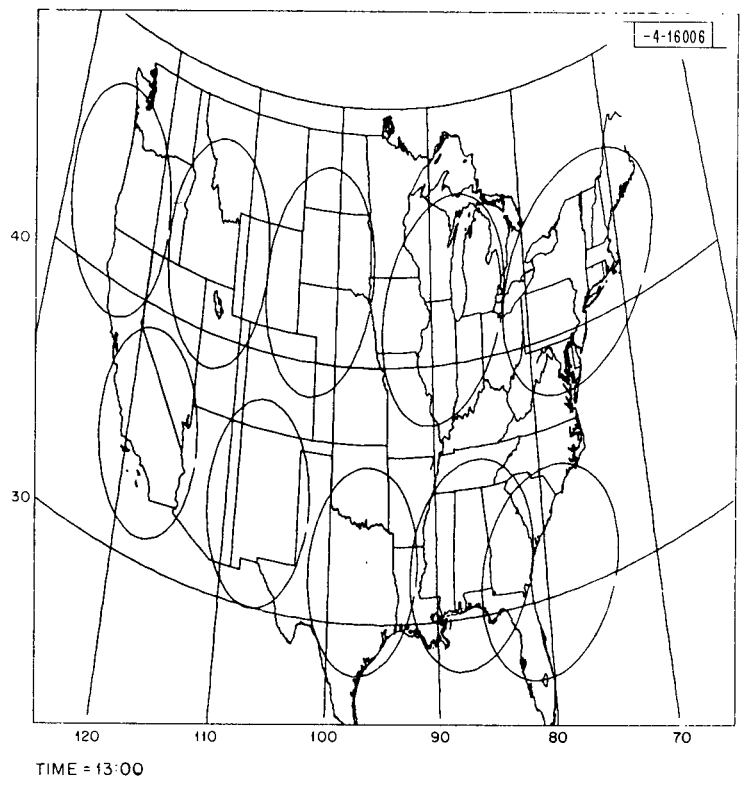

(m)

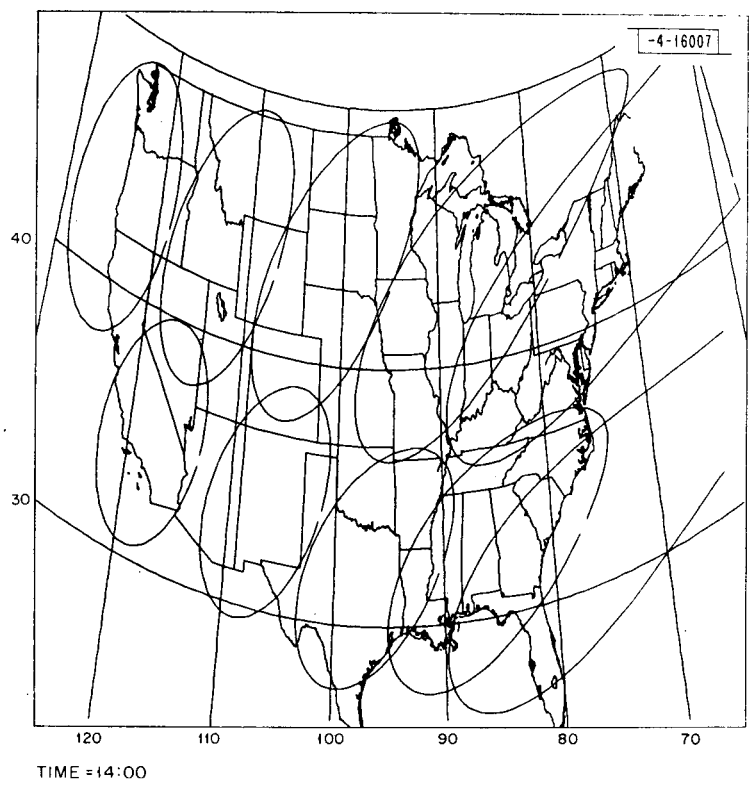

(n)

Fig. A.5. (continued).

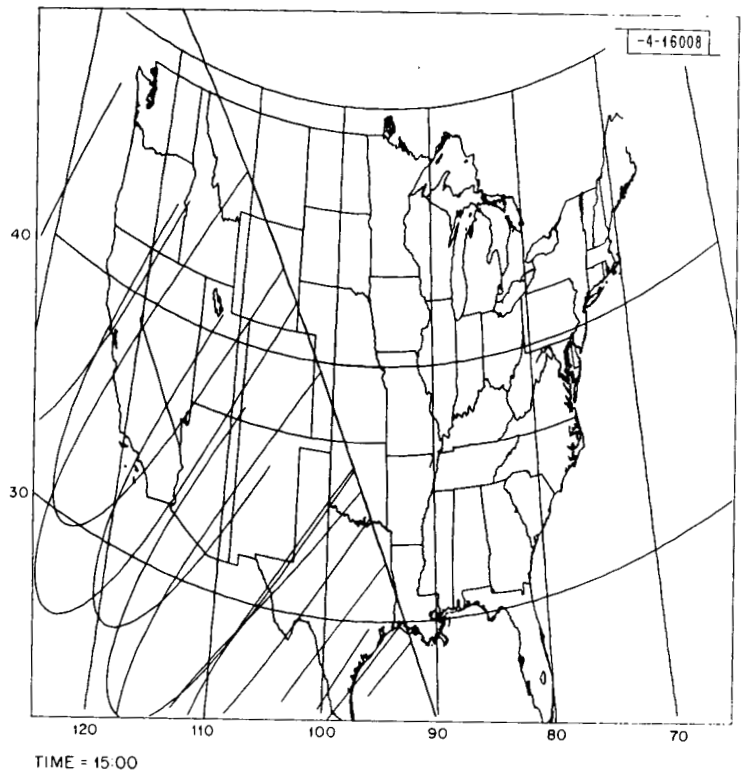

(o)

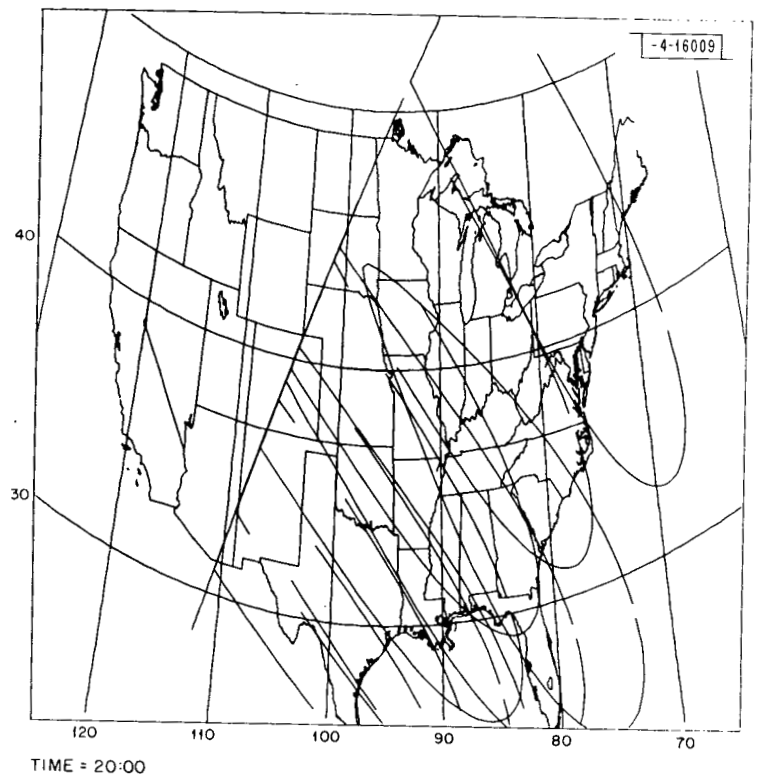

(p)

Fig. A.5. (continued).

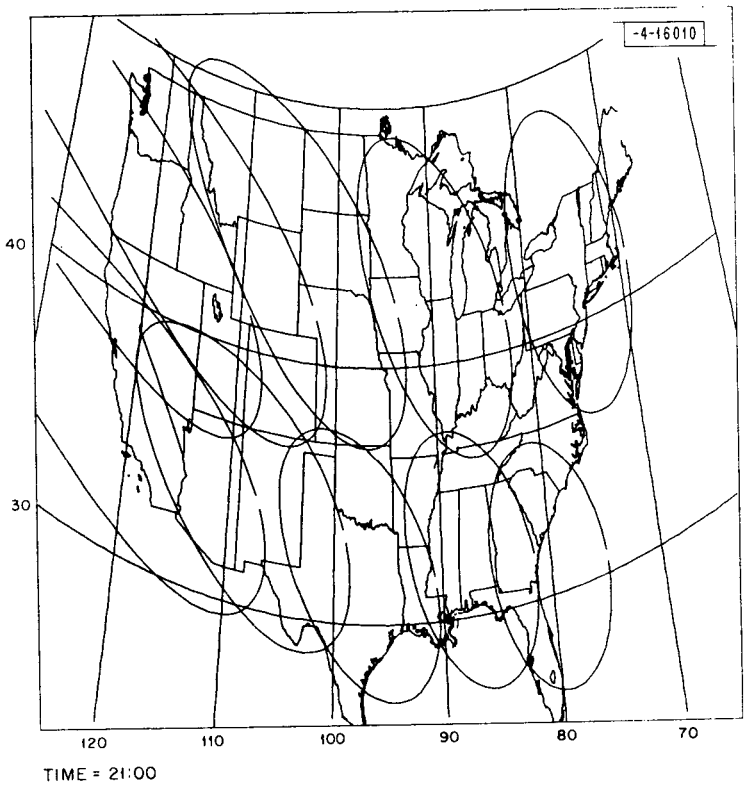

(q)

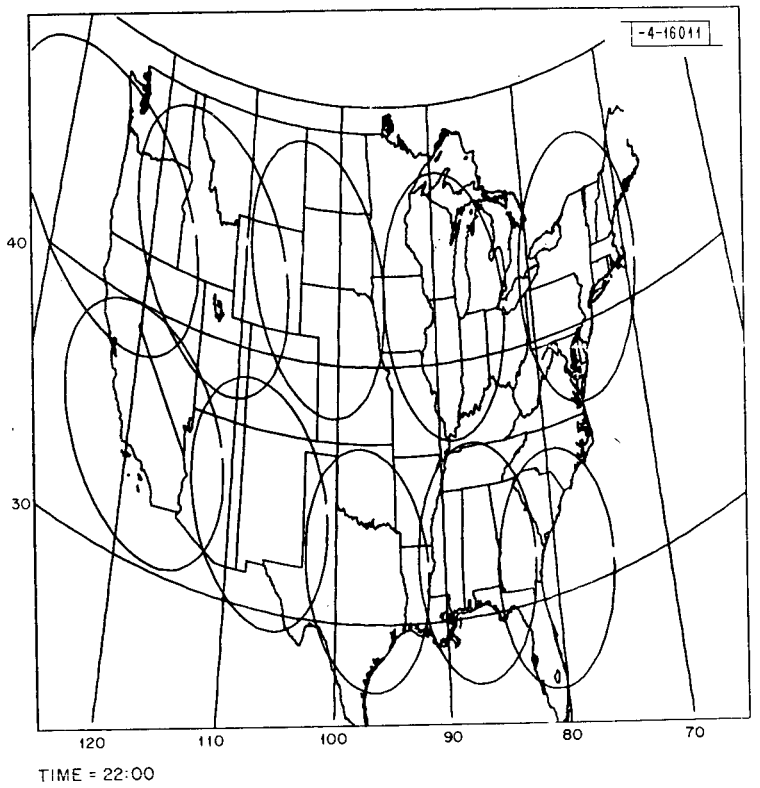

(r)

Fig. A.5. (continued).

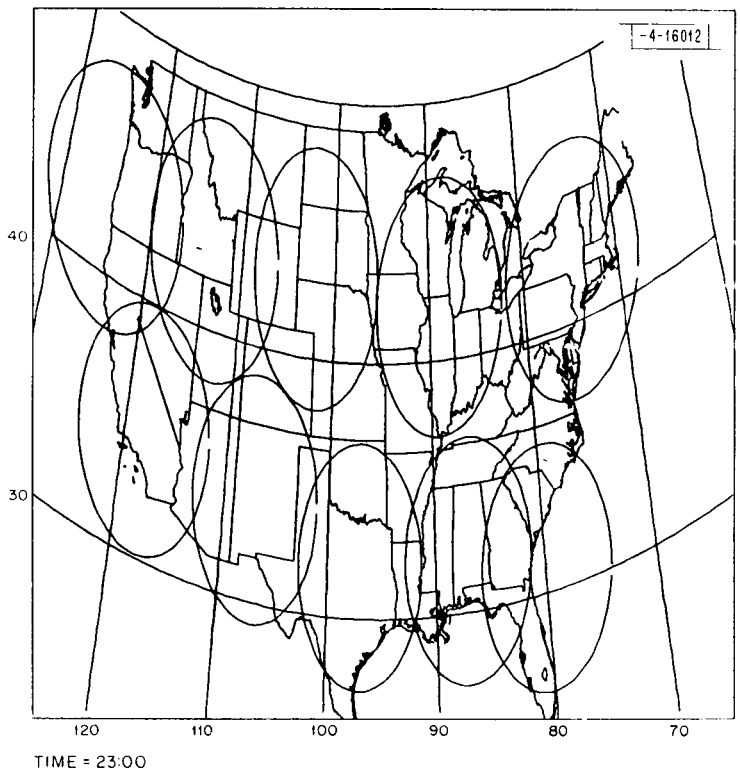

(s)

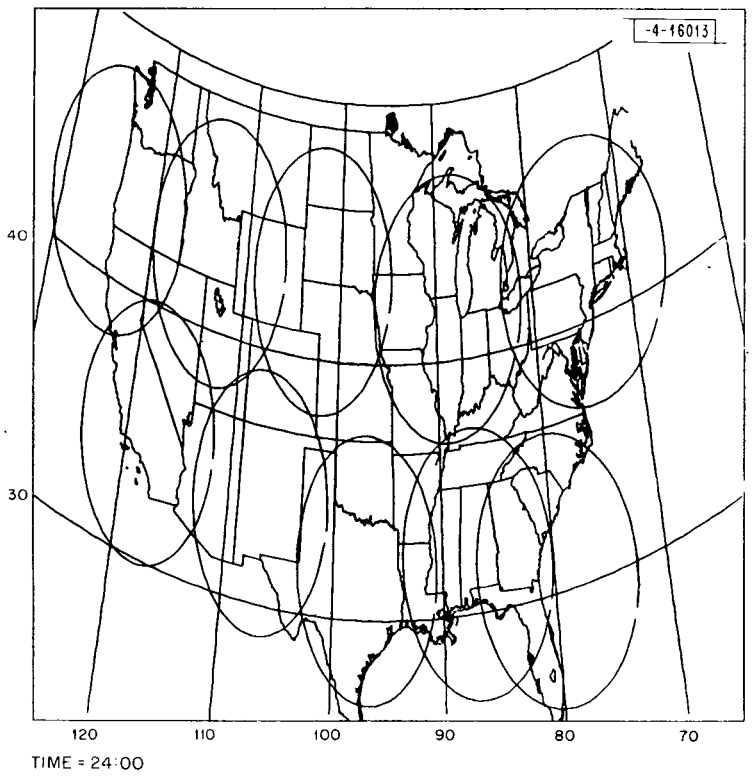

(t)

Fig. A.5. (continued).

APPENDIX B

AN UPPER BOUND TO ACQUISITION MISS PROBABILITY

In this appendix, we derive an upper bound to P_M, the probability that a given aircraft is "missed" on acquisition. A miss occurs if an incorrect TOA quadruplet is supplied to the aircraft's track file by the acquisition subsystem. The derivation carried out assumes; (1) the constellation employs the minimum number of satellites, 4; (2) the effect of mutual interference is the same as that of an equivalent power in-band white Gaussian noise source at the receiver input; (3) during acquisition the matched filter-envelope detector output samples are taken at the DPSK chip rate.

In carrying out the derivation we ignore the effect of phantom signatures. These arise when pulses from different received signatures combine and appear to constitute a valid signature, which however, is not present at the receiver at the indicated TOA. The contribution of such phantom signatures to P_M is believed to be quite small. Phantom signatures do not occur when single pulse aircraft signatures are employed.

The nomenclature to be used in the derivation is introduced below.

δ = maximum TOA difference between retransmissions of a given signature from two different satellites

α = update period

τ_c = DPSK chip duration

p_f = false alarm probability per matched filter-envelope detector sample

p_d = detection probability per matched filter-envelope detector sample*

$Q(\cdot,\cdot)$ = the Marcum Q function

*These are defined relative to the binary decision test performed on acquisition.

Consider the acquisition of a given aircraft transmitting a P pulse signature. The pulses in a P pulse signature are labelled A_1, A_2,...,A_p. Let the TOA of pulse A_i retransmitted from the master satellite be t_i. Assume that the three remaining satellites are labelled; SAT(1), SAT(2), SAT(3). For the aircraft which is to be acquired we will obtain an upper bound to P_M by lower bounding the probability of the event complementary to a "miss," which is a correct acquisition.

For the given aircraft to be correctly acquired it is sufficient that the following four conditions are satisfied:

(1) The pulses A_1,...,A_p retransmitted from the master satellite are all detected during the acquisition period.

(2) None of the master satellite matched filter-envelope detector samples taken from the A_1 pulse matched filter generate a false alarm during the acquisition period.

(3) The pulses A_1,...,A_p retransmitted from SAT(i); i=1,2,3, are all detected during the acquisition period.

(4) None of the SAT(i); i=1,2,3, matched filter-envelope detector samples taken from the pulse A_1 matched filter in the interval $[t_1-\delta, t_1+\delta]$ generate a false alarm.

Conditions (1), (2) and (3) are self-explanatory. Condition (4) is merely a check on the clustering of the A_1 pulse TOA's. If they do not lie within the specified interval, then the aircraft position computed from these TOA's would be an impossible one. A similar check could be made on the succeeding pulses as well, but the A_1 check should be sufficient to weed out most of the

phantom signatures or highly erroneous TOA quadruplets. Those which do pass will subsequently be eliminated by the acquisition subsystem.

Conditions (1)-(4) are expressed mathematically in terms of the following event definitions.

$$C_o = \left\{ \begin{array}{l} \text{For the master satellite receiver outputs, the pulses} \\ A_1,\ldots,A_P, \text{ are declared present at the correct pulse} \\ \text{TOA's during the acquisition period.} \end{array} \right\}$$

$$C_i = \left\{ \begin{array}{l} \text{For the SAT (i) receiver outputs, the pulses } A_1,\ldots,A_P \\ \text{are declared present at the correct pulse TOA's during} \\ \text{the acquisition period.} \end{array} \right\}$$

$$C_4 = \left\{ \begin{array}{l} \text{For the master satellite receiver output corresponding} \\ \text{to pulse } A_1, \text{ none of the } (\frac{\alpha}{\tau_c} - 1) \text{ receiver samples} \\ \text{examined during the acquisition period generate a pulse} \\ \text{false alarm.} \end{array} \right\}$$

$$B_i = \left\{ \begin{array}{l} \text{For the SAT(i) receiver output corresponding to pulse} \\ A_1; \text{ none of the } \frac{2\delta}{\tau_c} \text{ receiver samples examined in the} \\ \text{interval } [t_1 - \delta, t_1 + \delta] \text{ generate a pulse false alarm.} \end{array} \right\}$$

Correct acquisition includes the intersection of all these events. Thus, we have:

$$\{\text{correct acquisition}\} \supset C_o \bigcap_{i=1}^{3} C_i \bigcap C_4 \bigcap_{j=1}^{3} B_j \qquad \text{(B-1)}$$

$$\text{Prob}\{\text{correct acquisition}\} \geq \text{Prob}\{C_o\} \; (\text{Prob}\{C_1\})^3 \; \text{Prob}\{C_4\} \; (\text{Prob}\{B_1\})^3 \qquad \text{(B-2)}$$

The event probabilities are

$$\begin{aligned} \text{Prob } (C_o) &= p_d^{\,P} \\ \text{Prob } (C_1) &= p_d^{\,P} \\ \text{Prob } (C_4) &= (1 - p_f)^{\frac{\alpha}{\tau_c} - 1} \\ \text{Prob } (B_1) &= (1 - p_f)^{\frac{2\delta}{\tau_c} - 1} \end{aligned} \tag{B-3}$$

By applying (B-3) to (B-2), the following bound is obtained.

$$\text{Prob } \{\text{correct acquisition}\} \geq p_d^{\,4P} (1 - p_f)^{\frac{\alpha+6\delta}{\tau_c}} \tag{B-4}$$

We now invoke the assumption that the mutual interference has the same effect as an equivalent power in-band white Gaussian noise source. For the matched filter-envelope detector in this evironment, p_d and p_f are related (through the choice of detection threshold) as follows:

$$P_d = Q\left(\sqrt{\frac{2E_p}{N_{eff}}}, \sqrt{-2 \ln p_f}\right) \tag{B-5}$$

In (B-5), E_p/N_{eff} is the pulse energy-to-noise power density ratio. N_{eff} is the sum of the power densities of the receiver noise and the equivalent noise power density of the mutual interference.

Applying (B-5) to (B-4) brings

$$\text{Prob}\{\text{correct acquisition}\} \geq (1 - p_f)^{\alpha + \frac{6\delta}{\tau_c}} \left(Q\left[\sqrt{\frac{2E_p}{N_{eff}}}, \sqrt{-2 \ln p_f} \right] \right)^{4P} \quad \text{(B-6)}$$

The false alarm probability (equivalently, the detection threshold) can be varied to maximize the right hand side of (B-6). Since a miss is the complement of correct acquisition, the following upper bound is obtained:

$$P_M \leq 1 - \max_{p_f} \left\{ (1 - p_f)^{\alpha + \frac{6\delta}{\tau_c}} \left(Q\left[\sqrt{\frac{E_p}{N_{eff}}}, \sqrt{-2 \ln p_f} \right] \right)^{4P} \right\} \quad \text{(B-7)}$$

The bound (B-7) is used in Section 4.4 in studying the acquisition performance of systems employing RAST.

APPENDIX C

TIME OF ARRIVAL ESTIMATION IN THE PRESENCE OF MUTUAL INTERFERENCE

In this appendix we consider the problem of estimating the time of arrival of a PSK signal in the presence of both white Gaussian noise and the mutual interference created by other received signals of similar form. In previous analyses of this problem the effect of mutual interference has been assumed to be the same as that of an equivalent power in-band white Gaussian noise source. We depart from this assumption and instead model the interference as a filtered Poisson process. Special assumptions concerning the nature of the interfering waveforms are made which permit the development of a useful lower bound to the mean squared error in the TOA estimate.

The results are directly applicable to the problem of estimating the arrival time of a single pulse PSK signature that might be used in a system employing RAST. This signature type was described in Section 2 of this report. In the final section of this appendix, the results are appropriately modified so that they can be used for TOA error analysis of multiple pulse signatures as well.

C.1 WAVEFORM AND INTERFERENCE PROCESS MODELS

Each signal under consideration consists of a number of pulses, each of which is binary PSK modulated. Each pulse is composed of n binary chips. We assume that the chips in each pulse are obtained by random selection, i.e., each chip has phase angle 0° or 180° with equal probability. This model represents the general RAST signature. Such a model is not unreasonable; it has been known

for some time that single pulse PSK modulated signals constructed in this manner can have favorable auto-and crosscorrelation properties.

Single pulse signatures of this type have the following simple mathematical representation. Let $P(\cdot)$ denote a unit energy chip waveform (of duration τ_c), and let a_i denote the i-th chip amplitude ($a_i = \pm 1$). Then

$$S(t) = \sqrt{\frac{E}{n}} \sum_{i=1}^{n} a_i P(t - i\tau_c) \qquad (C\text{-}1)$$

E represents the total energy of S(t).

The phase angle of the received pulse is assumed to be random and uniformly distributed. The receiver consists of a matched filter-envelope detector. The receiver input contains the desired signal, white Gaussian noise of spectral density N_o W/Hz (single-sided) and a number of interfering signals which are also PSK pulses modulated by different binary codes. Before proceeding with the TOA error analysis it is necessary to make explicit the assumptions concerning the interference process.

1. The phase angles of the received pulses are statistically independent (uniformly distributed) random variables.

2. The interfering signals arrive independently at the matched filter receiver. Their arrival times are described by a Poisson process. The arrival rate function (μ) which statistically characterizes the process is assumed to be constant. For application to RAST, its value is the number of signals transmitted to the receiver divided by the transmission period; this is equivalent to the number of aircraft serviced/beam/sec.

3. The average received energy per interfering signal is λE. By varying λ we can study the TOA estimation accuracy for signals which are disadvantaged relative to the interfering signals. For simplicity we assume that each interfering signal has the average energy λE.

C.2 TIME OF ARRIVAL ESTIMATION ERROR: SINGLE PULSE

We begin the analysis by considering the interval of observation. The desired signal is assumed to have a time of arrival, τ, which lies in the interval $I = [-T_o/2, T_o/2]$ (the a priori uncertainty interval). The receiver output is observed over an interval including I for the purpose of estimating τ. In addition to the desired signal and the Gaussian noise, the receiver output contains contributions from a number of interfering signals. Let T_s denote the signal duration ($T_s = n\tau_c$). Only those signals which arrive during the interval $[-(T_o/2 + T_s), (T_o/2 + T_s)]$ contribute interference within the uncertainty interval I. Furthermore, only those that arrive within $\pm T_s$ sec of the desired signal arrival time will contribute interference to the mainlobe of the matched filter output. We note that when $T_o << T_s$, almost all the signals which contribute to the receiver output (within I) can be expected to overlap the mainlobe output. This would not be true if $T_o >> T_s$, but since we shall primarily be interested in how the interfering signals perturb the mainlobe of the output signals, we assume that the interference signals of concern are those which arrive within an interval of duration $2T_s$, centered at τ.

Let us look at the receiver output conditioned upon the arrival of exactly m interfering signals within $[-T_s + \tau, T_s + \tau]$. For convenience, it is assumed that their arrival times differ from that of the desired signal by an integral

number of chip durations. Let the filter output corresponding to the i-th interference signal at time τ be $\sqrt{\lambda E}\, y_i$*, and define

$$x = \sum_{i=1}^{m} y_i \qquad \text{(C-2)}$$

The total filter output at the signal arrival time is the sum of the desired signal autocorrelation mainlobe (amplitude $\sqrt{E}$) and the interference (amplitude $\sqrt{\lambda E}\, x$). The noise output is a Gaussian random variable of zero mean and variance $N_0/2$.

We will lower bound the worst case mean squared error in estimating the desired signal time of arrival, τ, using a method originally due to Ziv and Zakai.[23] Further developments of this technique are reported in Orr and Yates.[17] The essential concept of the Ziv-Zakai bound is that the mean squared TOA error ($\overline{e^2}$) can be bounded in terms of the error probability for a related binary hypothesis testing problem. The specific form of the bound is

$$\overline{e^2} \geq \sup_{0 \leq \Delta \leq T_0} \frac{\Delta^2}{4} P_e(\Delta) \qquad \text{(C-3)}$$

where $P_e(\Delta)$ is the minimum error probability for the decision problem in which the desired signal is transmitted at either time t_1 or time t_2 (with equal probability), where $t_1, t_2 \in [-T_0/2, T_0/2]$, and $|t_1 - t_2| = \Delta$.† This bounding technique is applied to the present problem by first computing a lower bound to the conditional mean squared error, $e^2(m,x)$. This is the mean squared estimation error conditional on the values of m and x. When the conditioning

*The matched filter impulse response is normalized to have unit energy.

†For this form of the bound to apply, it must be true, as it is in the present case, that $P_e(\Delta)$ is a function of t_1 and t_2 only through their absolute difference Δ.

is removed by averaging over the joint probability density of those variables, the result remains a lower bound to the TOA error, $\overline{e^2}$.

In applying the bound, we ignore the presence of intefering signals at all times other than those within $\pm\tau_c$ of the desired signal arrival time. This is consistent with obtaining the desired lower bound. The interference overlapping the mainlobe is represented as an additional signal component superimposed on the desired signal.

It is mathematically convenient to carry out the Ziv-Zakai analysis in terms of the known phase, rather than the random phase, channel model (replacing the matched filter-envelope detectors with matched filters). Since the error probability for the known phase case is the smaller of the two, the result is still a lower bound to $\overline{e^2}$. This convenience weakens the bound by only a negligible amount since the two error probabilities are so nearly equal.

The evaluation of $e^2(m,x)$ requires treatment of two separate cases. The first case is that in which the autocorrelation mainlobe and the interference outputs combine destructively. We interpret this to mean that the matched filter output is negative at the true arrival time. This occurs only if $x < -1/\sqrt{\lambda}$. We treat this case as though the signal were transmitted with no energy. Then, of course, the optimum receiver for the decision problem merely makes a random choice, and $P_{e\ m,x}(\Delta) = \frac{1}{2}$ for all Δ. The corresponding error bound is

$$e^2(m,x) = \frac{T_o^2}{8} \quad ; \quad x \leq 1/\sqrt{\lambda} \tag{C-4}$$

The second case is that in which the signal plus interference is positive at the arrival time. It is treated as though the signal energy is $E(1 + \sqrt{\lambda}x)^2$.

The error probability for the second case is

$$P_{e|m,x}(\Delta) = Q\left[(1 + \sqrt{\lambda}\, x)\sqrt{(1 - \rho_\Delta)\frac{E}{N_o}}\right] \quad ; \quad x \geq -1/\sqrt{\lambda} \qquad (C\text{-}5)$$

where $Q(\cdot)$ represents the Gaussian probability integral

$$Q(y) = \frac{1}{\sqrt{2\pi}} \int_y^\infty du\ e^{-u^2/2} \qquad (C\text{-}6)$$

and ρ_Δ is the autocorrelation function of the received signal-plus-interference process. The error bound corresponding to this cannot be calculated unless the form of ρ_Δ is known.

Because the chips in the PSK pulse signal are chosen randomly we can assume with some justification that the pulse signal has a narrow autocorrelation main-lobe and low sidelobes. Except for the sidelobes, the PSK pulse autocorrelation function resembles the autocorrelation function of the chip waveform. This is the autocorrelation function which would result if the transmitted waveform actually consisted of a single chip of energy E, rather than n consecutive chips, each of energy E/n. We choose this single-chip representation for ρ_Δ and ignore the effects of the (low) sidelobes on the actual autocorrelation function.

Let us assume that the chip waveform, P(t), is an approximately rectangular shaped pulse of duration τ_c and finite mean squared bandwidth β^2.* The auto-correlation function of such a pulse can be approximated as

*If, for example, the chip waveform is trapezoidal with rise and fall times τ_r, then $\beta^2 = 2/\tau_r\tau_c$.

$$\rho_\Delta \simeq \begin{cases} 1 - \frac{1}{2}\beta^2\Delta^2 \; ; & |\Delta| \leq \frac{2}{\beta^2\tau_c} \\ 1 - |\Delta|/\tau_c \; ; & \frac{2}{\beta^2\tau_c} \leq |\Delta| \leq \tau_c \\ 0 \; ; & \tau_c \leq |\Delta| \end{cases} \tag{C-7}$$

Equation (C-7) can be applied to $P_{e|m,x}(\Delta)$ given by (C-5). The resulting Ziv-Zakai error bound for this case has in fact been shown to be[17]

$$e^2(m,x) \geq \max \{\hat{B}_i, \hat{B}_e\} \tag{C-8}$$

where

$$\hat{B}_i = \begin{cases} \left(\frac{\tau_c}{2}\right)^2 Q\left[(1 + \sqrt{\lambda}\, x)\sqrt{\frac{E}{N_o}}\right]; & (1 + \sqrt{\lambda}x)^2 \frac{E}{N_o} \leq \gamma_1 \quad \text{(C-9a)} \\ \frac{0.1\,\tau_c^2}{(1 + \sqrt{\lambda}x)^4 (\frac{E}{N_o})^2} \; ; & \gamma_1 \leq (1 + \sqrt{\lambda}x)^2 \frac{E}{N_o} \leq \gamma_2 \quad \text{(C-9b)} \\ \frac{0.083}{(1 + \sqrt{\lambda}x)^2 (\frac{E}{N_o})\beta^2} \; ; & \gamma_2 \leq (1 + \sqrt{\lambda}x)^2 \frac{E}{N_o} \quad \text{(C-9c)} \end{cases}$$

and

$$\hat{B}_e = \left(\frac{T_o}{2}\right)^2 Q\left[(1 + \sqrt{\lambda}x)\sqrt{\frac{E}{N_o}}\right] \tag{C-10}$$

The thresholds in the formula for $\hat{B}_i$ are given by*

$$\gamma_1 = 3.27 \tag{C-11}$$

$$\gamma_2 = 1.14(\beta\tau_c)^2$$

The form of this result is discussed at length in Orr and Yates.[17] To summarize briefly, the three regions of $\hat{B}_i$ (C-9) correspond to: (a) errors of magnitude comparable to the chip width (low SNR); (b) errors around the autocorrelation peak when the waveform is indistinguishable from that of a square pulse (intermediate SNR); and (c) local errors about the autocorrelation peak, i.e., the Cramer-Rao bound (high SNR). The external bound, $\hat{B}_e$ (C-10), accounts for large anomolous errors due to noise peaks outside the autocorrelation mainlobe.

Equation (C-9) can be simplified somewhat by assuming that $T_o > \tau_c$ for the cases of interest, and by replacing the square pulse region of the $\hat{B}_i$ formula with the Cramer-Rao portion. The latter step weakens the bound only slightly.

$$e^2(m,x) \geq \max \begin{cases} \left(\frac{T_o}{2}\right)^2 Q\left[(1+\sqrt{\lambda}x)\sqrt{\frac{E}{N_o}}\right] & ; \quad x \geq -1/\sqrt{\lambda} \qquad \text{(C-12a)} \\ \dfrac{0.083}{(1+\sqrt{\lambda}\,x)^2 \dfrac{E}{N_o}\,\beta^2} & \qquad \text{(C-12b)} \end{cases}$$

*Note that $\gamma_2 > \gamma_1$, since the time-bandwidth product $\beta\tau_c$ must exceed π.

Equations (C-4) and (C-12) provide the necessary lower bounds to $e^2(m,x)$. In order to carry out the average over x, one must know the value of x at which the two expressions in (C-12) cross. By inspecting the formulas one can see that the solution is of the form

$$(1 + \sqrt{\lambda}x)^2 \frac{E}{N_0} = f(\beta T_0) \tag{C-13}$$

where $f(\cdot)$ is a function only of the time-bandwidth product βT_0. Figure C.1 shows the value of E/N_0 (called the threshold signal-to-noise ratio) at which the expressions cross in the absence of mutual interference (i.e., $\lambda = 0$). The solution for x is readily obtained from this graph for any nonzero value of λ.

Let us first restrict attention to values of E/N_0 which would be above threshold in the absence of mutual interference. For these cases, the value of x at which crossover occurs must be negative. Then (C-12a) will dominate at small E/N_0, and (C-12b) at large E/N_0. We will further underbound $e^2(m,x)$ if we arbitrarily set the crossover point at x=0. Using this procedure, we obtain the following bound on $e^2(m,x)$:

$$e^2(m,x) \geq \begin{cases} \dfrac{T_0^2}{8} & ; \quad x \leq -\dfrac{1}{\sqrt{\lambda}} \\ \dfrac{T_0^2}{4} Q\left[(1 + \sqrt{\lambda}\, x)\sqrt{\dfrac{E}{N_0}}\right] & ; \quad -\dfrac{1}{\sqrt{\lambda}} \leq x \leq 0 \\ \dfrac{0.083}{(1 + \sqrt{\lambda}\, x)^2 (\frac{E}{N_0})\, \beta^2} & ; \quad 0 \leq x < \infty \end{cases} \tag{C-14}$$

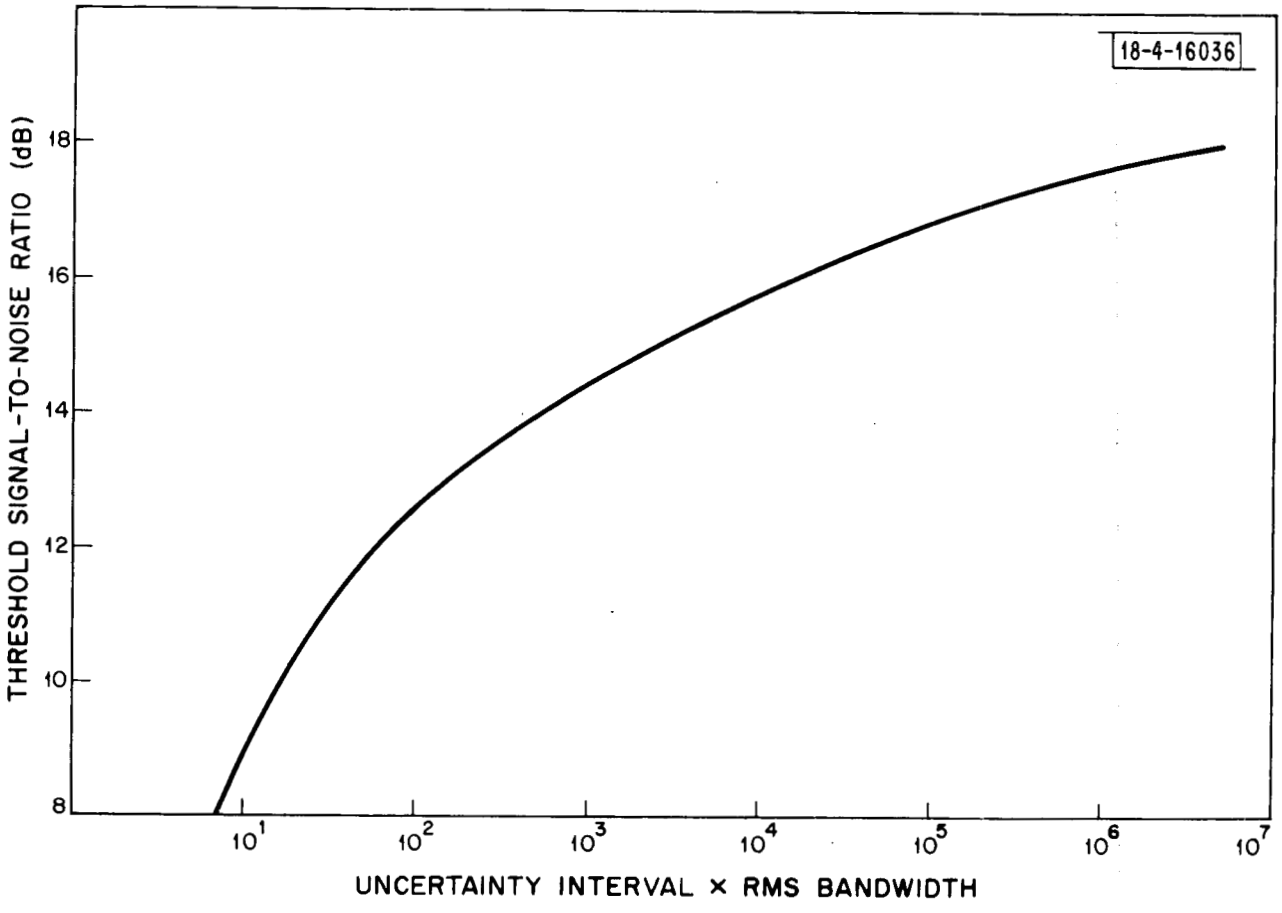

Fig. C.1. Threshold signal-to-noise ratio vs βT_0.

If, on the other hand, E/N_o is below threshold, the crossover point is at a positive value of x. In that case we further underbound $e^2(m,x)$ by ignoring the Cramer-Rao portion of the bound:

$$e^2(m,x) \geq \begin{cases} \frac{T_o^2}{8} & ; \quad -\infty < x \leq -1/\sqrt{\lambda} \\ \frac{T_o^2}{4} \, Q\left[(1 + \sqrt{\lambda}\, x)\sqrt{\frac{E}{N_o}}\right] & ; \quad -1/\sqrt{\lambda} \leq x < \infty \end{cases} \qquad \text{(C-15)}$$

E/N_o below threshold

Now we compute the expectation of $e^2(m,x)$ with respect to x for a non-zero value of m. For a fixed value of m, x is a linearly scaled and translated binomial random variable. It is essentially equal to

$$x = \frac{1}{n} \sum_{i=1}^{m} \sum_{j=1}^{n} a_{ij} \qquad \text{(C-16)}$$

where $a_{ij} = \pm 1$ with equal probability. Thus $\bar{x} = 0$ and $\overline{x^2} = \frac{m}{n}$*. Since x is the sum of mn identically distributed variables, where n will be reasonably large ($\simeq$500 in the cases of interest), we can assume that x is a Gaussian random variable.

Given this assumption about x, the average of $e^2(m,x)$ can be lower bounded by averaging the lower bounds (C-14 and C-15) with respect to x. In the former case (E/N_o above threshold), the average leads to three integrals (I_1, I_2 and I_3),

*Equation (C-16) is strictly true only if all m interfering signals overlap the desired signal completely. For partial overlaps, there are fewer summands and the variance of x exceeds m/n. This minimum variance assumption for x is consistent with obtaining a lower bound to $\overline{e^2}$.

the resultant lower bound being the sum of these. Each integral corresponds to one of the regions of x indicated in (C-14).

Integral I_1:

$$I_1 = \int_{-\infty}^{-1/\sqrt{\lambda}} dx \, \frac{T_o^2}{8} \, \frac{1}{\sqrt{2\pi m/n}} \, e^{-\frac{nx^2}{2m}} \qquad \text{(C-17)}$$

$$= \frac{T_o^2}{8} \, Q\left[\sqrt{\frac{n}{m\lambda}}\right]$$

Integral I_2:

$$I_2 = \int_{-1/\sqrt{\lambda}}^{0} dx \, \frac{T_o^2}{4} \, Q\left[\left(1+\sqrt{\lambda}x\right)\sqrt{\frac{E}{N_o}}\right] \, \frac{e^{-\frac{nx^2}{2m}}}{\sqrt{2\pi m/n}}$$

$$= \frac{T_o^2}{4} \int_{-\sqrt{n/m\lambda}}^{0} du \, Q\left[\left(1+\sqrt{\frac{m\lambda}{n}}\,x\right)\sqrt{\frac{E}{N_o}}\right] \, \frac{e^{-\frac{u^2}{2}}}{\sqrt{2\pi}} \qquad \text{(C-18)}$$

$$= \frac{T_o^2}{4} \int_{-\sqrt{n/m\lambda}}^{0} du \int_{\left(1+\sqrt{\frac{m\lambda}{n}}\right)\sqrt{\frac{E}{N_o}}}^{\infty} dv \, \frac{e^{-\frac{(u^2+v^2)}{2}}}{2\pi}$$

The formula for I_2 has been converted to an integral of a standardized two dimensional Gaussian variable over a portion of the plane. Figure C.2a indicates the integration region. I_2 can be lower bounded by diminishing the integration region as indicated in the figure. Using that region the following is obtained directly:

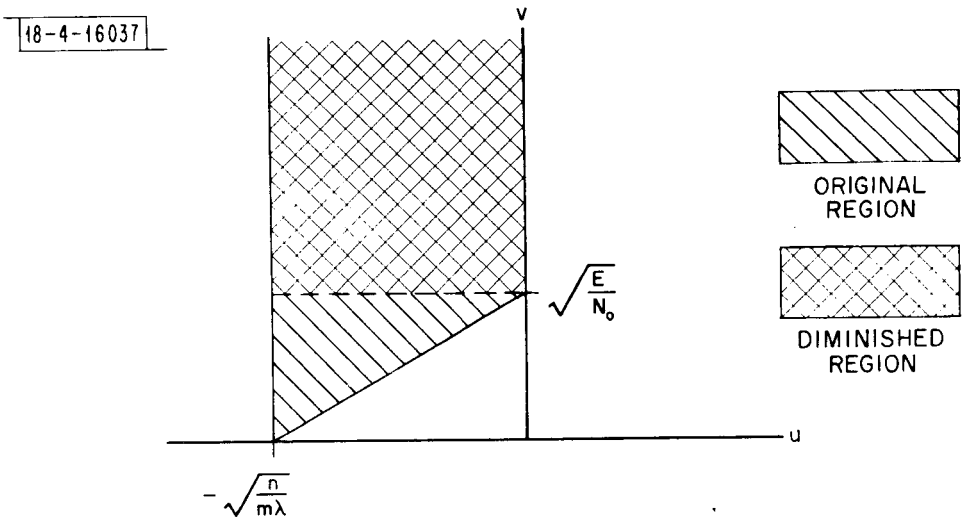

(a)

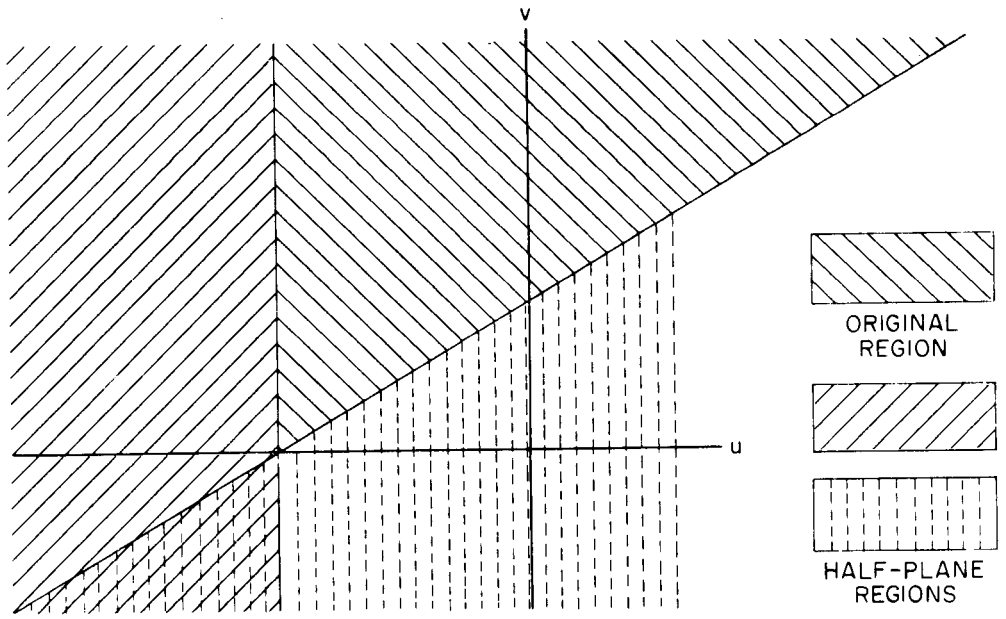

(b)

Fig. C.2. Integration regions for I_2 and I_2'.

$$I_2 \geq \frac{T_o^2}{4} Q\left(\sqrt{\frac{E}{N_o}}\right) \left[\frac{1}{2} - Q\left(\sqrt{\frac{n}{m\lambda}}\right)\right] \tag{C-19}$$

Integral I_3:

$$I_3 = \int_0^\infty dx \frac{0.083 \; e^{-\frac{nx^2}{2m}}}{\sqrt{2\pi m/n}\left(\frac{E}{N_o}\right)\beta^2(1+\sqrt{\lambda}\,x)^2} = \frac{0.083}{(E/N_o)\,\beta^2} \int_0^\infty \frac{du}{\sqrt{2\pi}} \frac{e^{-u^2/2}}{\left(1+\sqrt{\frac{m\lambda}{n}}\,u\right)^2} \tag{C-20}$$

It is easy to prove that the denominator of the latter integral can be upper and lower bounded to within a factor of 2 as follows:

$$\frac{1}{2\left(1+\frac{m\lambda}{n}u^2\right)} \leq \frac{1}{\left(1+\sqrt{\frac{m\lambda}{n}}\,u\right)^2} \leq \frac{1}{1+\frac{m\lambda}{n}u^2} \tag{C-21}$$

Using the lower bound in the integral (C-20), one obtains:

$$\int_0^\infty \frac{du}{\sqrt{2\pi}} \frac{e^{-u^2/2}}{\left(1+\sqrt{\frac{m\lambda}{n}}\,u\right)^2} \geq \int_0^\infty \frac{du}{\sqrt{2\pi}} \frac{e^{-u^2/2}}{2\left(1+\frac{m\lambda}{n}u^2\right)} = \frac{1}{2} \frac{\pi n}{2m\lambda} e^{\frac{n}{2m\lambda}} Q\left(\sqrt{\frac{n}{m\lambda}}\right)^* \tag{C-22}$$

*The integral is given on p. 338 of Gradshteyn and Ryzhik.[24]

Using the following standard lower bound to the $Q(\cdot)$ function,

$$Q(x) > \frac{2e^{-x^2/2}}{\sqrt{2\pi}\left(x + \sqrt{x^2 + 4}\right)} \tag{C-23}$$

(C-22) can be further simplified. The resulting bound on I_3 is

$$I_3 \geq \frac{0.0415}{(E/N_o)\beta^2\left(1 + \sqrt{1 + \frac{4m\lambda}{n}}\right)} \tag{C-24}$$

The condition under which I_3 makes a significant contribution to the total bound is when $m\lambda/n$ is small. In that case the upper bound in (C-21) is a more accurate approximation than is the lower bound. Therefore, we can increase (C-24) by a factor of 2:

$$I_3 \geq \frac{0.083}{(E/N_o)\,\beta^2\left(1 + \sqrt{1 + \frac{4m\lambda}{n}}\right)} \tag{C-25}$$

Summing I_1, I_2 and I_3 yields

$$\begin{aligned} e^2(m) &= E_x[e^2(m,x)] \\ &\geq \frac{T_o^2}{8}\left\{Q\left(\sqrt{\frac{E}{N_o}}\right) + Q\left(\sqrt{\frac{n}{m\lambda}}\right)\left[1 - 2Q\left(\sqrt{\frac{E}{N_o}}\right)\right]\right\} \\ &+ \frac{0.083}{(E/N_o)\,\beta^2\left(1 + \sqrt{1 + \frac{4m\lambda}{n}}\right)} \quad ; \; E/N_o \text{ above threshold} \end{aligned} \tag{C-26}$$

For E/N_o below threshold, the average consists of two integrals. The first is I_1, which has been evaluated in (C-17). The second is a modification of I_2 (call it I_2'):

$$I_2' = \int_{-1/\sqrt{\lambda}}^{\infty} dx \quad \frac{T_o^2}{4} \; Q\left[(1+\sqrt{\lambda}\, x)\sqrt{\frac{E}{N_o}}\right] \; \frac{e^{-\frac{mx^2}{2m}}}{\sqrt{2\pi}} \tag{C-27}$$

$$= \frac{T_o^2}{4} \int_{-\sqrt{n/m\lambda}}^{\infty} du \quad \int_{(1+\sqrt{m\lambda/n}\, u)\sqrt{\frac{E}{N_o}}}^{\infty} dv \quad \frac{e^{-\frac{u^2+v^2}{2}}}{2\pi}$$

The integration region in the u,v coordinates is indicated in Fig. C.2 b. We lower bound I_2' by upper bounding the volume in the complement of the integration region. Specifically, we compute the two indicated half-plane volumes. This leads to

$$1 - I_2'/(T_o^2/4) \leq Q\left[\sqrt{\frac{n}{m\lambda}}\right] + Q\left[-\sqrt{\frac{E/N_o}{(E/N_o)(m\lambda/n) + 1}}\right] \tag{C-28}$$

or

$$I_2' \geq \frac{T_o^2}{4}\left\{Q\left[\sqrt{\frac{E/N_o}{(E/N_o)(m\lambda/n) + 1}}\right] - Q\left[\sqrt{\frac{n}{m\lambda}}\right]\right\} \tag{C-29}$$

The bound on $e^2(m)$, $(I_1 + I_2')$, is

$$e^2(m) \geq \frac{T_o^2}{8}\left\{2Q\left[\sqrt{\frac{E/N_o}{(E/N_o)(m\lambda/n)+1}}\right] - Q\left[\sqrt{\frac{n}{m\lambda}}\right]\right\} \qquad \text{(C-30)}$$

When m = 0, we use the no-interference expressions, which are obtained from (C-12):

$$e^2(0) \geq \begin{cases} \frac{T_o^2}{4}\, Q\left(\sqrt{\frac{E}{N_o}}\right); & E/N_o \text{ below threshold} \\ \frac{0.83}{(E/N_o)\beta^2}; & E/N_o \text{ above threshold} \end{cases} \qquad \text{(C-31)}$$

What remains to be accomplished is the expectation of $e^2(m)$ with respect to m. We do not have a closed form expression for this average. It is indicated as a sum over the Poisson variable. Following the earlier discussion, we assume that m is Poisson with mean $\bar{m} = 2\mu T_s$:

$$\text{Prob}(m) = \frac{(2\mu T_s)^m}{m!}\, e^{-2\mu T_s} \qquad \text{(C-32)}$$

Then

$$\overline{e^2} \geq \sum_{m=0}^{\infty} \frac{(2\mu T_s)^m}{m!}\, e^{-2\mu T_s}\, e^2(m) \qquad \text{(C-33)}$$

The appropriate expressions are substituted in for $e^2(m)$, according to whether E/N_o exceeds threshold.

In order to apply these results to the RAST signature TOA analysis in Section 4 of the report, the calculation indicated in (C-33) is carried out using a partial sum of the first 40 terms of the summation.

C.3 TIME OF ARRIVAL ESTIMATION ERROR: MULTIPLE PULSE

Time of arrival estimation for a multiple pulse signature is accomplished by measuring the TOA of each individual pulse. A translated average of these estimates is used for the signature TOA. The presence of the additional pulses reduces the TOA error because of the averaging. However, in the mutual interference environment which we have described, there is the opportunity to incorrectly associate a received pulse with its parent signature and thereby make a large TOA error. We now show how to modify the preceding analysis to account for these two effects.

The receiver for a P-pulse signature has a filter matched to each of the pulses. In estimating the pulse TOA's, the output of each filter is examined over an interval of width T_o centered at the expected arrival time for that pulse. Each of these matched filter outputs may contain the desired pulse, interfering pulses from other signature arrivals and Gaussian noise. The particular pulse to which the filter is matched may also be contained in one of the interfering signatures. This is in contrast to the single pulse case, in which all signatures could be required to differ by some prescribed amount. Reception of a spurious pulse of this sort can cause a large TOA error if the desired pulse is masked. The effect of spurious pulses on the TOA error is analyzed as follows.

We assume that the spacing between signature pulses exceeds $(T_s + T_o)$. This guarantees that no more than one pulse of an interfering signature can

be contained in the arrival uncertainty window. Thus, each interfering pulse arrives independently of all others, and the Poisson arrival model which was used for single pulse signatures now applies directly to the multiple pulse problem.

A spurious pulse ambiguity results when one or more interfering pulses arrive within the uncertainty window, and at least one of them has the same waveform as the intended pulse. If the intended user is significantly disadvantaged in power relative to the average user, the receiver will almost always make its TOA estimate on the basis of the received energy of the spurious pulse. In order to be consistent with the assumptions leading to (C-33), the single pulse TOA error bound, we calculate the worst case error which can arise from spurious pulse receptions.

As a consequence of the Poisson arrival model, the arrival time of an interfering pulse is uniformly distributed throughout the observation interval. The resulting TOA estimate is assumed to be similarly distributed. The worst case error occurs when the intended pulse arrives at either endpoint of the observation interval; $\overline{e_a^2}$, the mean squared value of this error, is

$$\overline{e_a^2} = \frac{T_o^2}{3} \qquad \text{(C-34)}$$

Let q denote the probability that no spurious pulses are received within the uncertainty window corresponding to a given pulse. The mean squared TOA error for that pulse, $\overline{e_p^2}$, is bounded by

$$\overline{e_p^2} \geq q\,\overline{e^2} + (1 - q)\,\overline{e_a^2} \tag{C-35}$$

where $\overline{e^2}$ is the single pulse error given in (C-33). The calculation of q is straightforward. It will be done in terms of the signature arrival rate μ:

$$\mu = \frac{fN_T}{\alpha} \tag{C-36}$$

(the right hand side quantities are defined in Section 4.3).

Each interfering P-pulse signature may arrive so that any one of its P pulses overlaps the intended pulse window. Thus, the set of arrival times for which that signature contributes an interfering pulse has duration PT_o. The probability that exactly m such signatures arrive is

$$\text{Prob}\ (m) = \frac{(\mu PT_o)^m}{m!}\ e^{-\mu PT_o} \tag{C-37}$$

The probability that none of the overlapping pulses are identical to the intended pulse is $(1 - \frac{1}{N})^m$, where N is the size of the elementary pulse set. Thus, the probability of no spurious pulses is

$$q = \sum_{m=0}^{\infty} \frac{(\mu PT_o)^m}{m!}\ e^{-\mu PT_o} (1 - \frac{1}{N})^m$$

$$= e^{-\frac{\mu PT_o}{N}} \tag{C-38}$$

Then the per pulse TOA error is

$$\overline{e_p^2} = e^{-\frac{\mu P T_o}{N}} \overline{e^2} + \left(1 - e^{-\frac{\mu P T_o}{N}}\right) \frac{T_o^2}{3} \qquad \text{(C-39)}$$

Since the P intended pulse TOA's can be averaged in determining the signature TOA, the total error is

$$\varepsilon^2 = \frac{\overline{e_p^2}}{P} \qquad \text{(C-40)}$$

For small arrival rates, the single pulse term in (C-39) is dominant. For very large arrival rates, spurious pulses are a virtual certainty, and the $T_o^2/3$ dominates. The behavior at intermediate rates depends upon the threshold behavior of $\overline{\varepsilon^2}$ as a function of μ.

REFERENCES

1. "Final Report - Advanced Air Traffic Management System," Report C72-1206/201, Rockwell International Corporation, Anaheim, California (April 1973).

2. L. Schuchman, "The ASTRO-DABS Concept," Technical Report MTR-6287, MITRE Corporation, McLean, Virginia (November 1972).

3. "Advanced Air Traffic Management - System B Summary Report," MTR-6419 Series 1, MITRE Corporation, McLean, Virginia (June 1973), FAA-EM-73-10.

4. "Study and Concept Formulation of a Fourth Generation Air Traffic Control System," Vols. I-V, Report DOT-TSC-3601-1, Boeing Company, Renton, Washington (April 1972).

5. P. M. Diamond, "The Potential of a System of Satellites as a Part of an Air Traffic Control System," AGARD Conference Proceedings 105, p. 20-1 (June 1972).

6. D. D. Otten, "Study of a Navigation and Traffic Control Technique Employing Satellites," Vols. I-IV, Group Report 08710-6012-12000, TRW Systems, Redondo Beach, California (December 1967).

7. K. D. McDonald, "A Survey of Satellite-Based Systems for Navigation, Position Surveillance, Traffic Control and Collision Avoidance," Addendum to Proceedings of ION National Aerospace Meeting, Institute of Navigation, Washington, D.C. (March 1973).

8. R.S. Orr and K.S. Schneider, "Technical Assessment of Satellites for CONUS Air Traffic Control, Vol. I: Coordinated Aircraft-to-Satellite Techniques," Project Report ATC-26, Vol. I, Lincoln Laboratory, M.I.T. (31 January 1974), DOT/TSC-241-4.

9. H.B. Lee and B.B. Goode, "Technical Assessment of Satellites for CONUS Air Traffic Control, Vol. III: Satellite-to-Aircraft Techniques," Project Report ATC-26, Vol. III, Lincoln Laboratory, M.I.T. (19 February 1974), DOT/TSC-RA-3-8-3.

10. H.L. Gerwin and G.K. Campbell, "The Wrap Rib Parabolic Reflector Antenna," Report LMSC/A969503, Lockheed Missiles and Space Company, Sunnyvale, Calif.

11. H.B. Lee and A.E. Wade, "Improved Satellite Constellations for CONUS ATC Coverage," Project Report ATC-23, Lincoln Laboratory, M.I.T. (to be published).

12. I. G. Stiglitz, J. U. Beusch, A. E. Eckberg, and K. S. Schneider, "Concept Formulation Studies of the Surveillance Aspects of the Fourth Generation Air Traffic Control System," Project Report ATC-7, Lincoln Laboratory, M.I.T. (21 September 1971), DOT/TSC-241-1.

13. G. V. Colby and E. A. Crocker, "Final Report Transponder Test Program," Project Report ATC-9, Lincoln Laboratory, M.I.T. (12 April 1972), FAA-RD-72-30.

14. G. V. Colby and E. A. Crocker, "Transponder Frequency Drift During a 100 Microsecond Pulse Transmission," private communication.

15. H. D. Goldfein, "AATMS System 'A' Receiver Performance," private communication.

16. K. S. Schneider, I. G. Stiglitz, and A. E. Eckberg, "Surveillance Aspects of the Advanced Air Traffic Management System," Project Report ATC-10, Lincoln Laboratory, M.I.T. (22 June 1972), DOT/TSC-241-2.

17. R. S. Orr and R. D. Yates, "On the Estimation of the Arrival Time of Pulse Signals in Gaussian Noise," Technical Note 1974-13, Lincoln Laboratory, M.I.T. (to be published).

18. N. N. Rao, M. Y. Youakim and K. C. Yeh, "Feasibility Study of Correcting for Excess Time Delay of Transionospheric Navigational Ranging Signals," Technical Report 43, U. Illinois Ionosphere Radio Laboratory (July 1971), SAMSO TR 71-163.

19. B. Gold, et al., "The FDP, a Fast Programmable Signal Processor," IEEE Trans. Computers, Vol. C-20, No. 1, pp. 33-38,(January 1971).

20. H. L. Groginsky, "A Pipeline Fast Fourier Transform," IEEE Trans. Computers, Vol. C-19, No. 11, pp. 1015-1019 (November 1970).

21. B. Gold and T. Bially, "Parallelism in Fast Fourier Transform Hardware," IEEE Trans. Audio Electroacoust., Vol. AU-21, No. 1, pp. 5-16, (February 1973).

22. H. B. Lee, "Accuracy Limitations of Hyperbolic Multilateration Systems," Technical Note 1973-11, Lincoln Laboratory, M.I.T. (22 March 1973), DOT/TSC-241-3.

23. J. Ziv and M. Zakai, "Some Lower Bounds on Signal Parameter Estimation," IEEE Trans. Inform. Theory,. Vol. IT-15, No. 3, pp. 386-391 (May 1969).

24. I.S. Gradshteyn, and I. M. Ryzhik, Table of Integrals, Series and Products (Academic Press, New York and London, 1965).

ACKNOWLEDGEMENT

It is a pleasure to acknowledge the assistance of Frederick Zimnoch in assembling and running the programs which provided the satellite antenna coverage maps and data. Frances Chen also provided programming support for this effort. The authors especially acknowledge the guidance provided by Dr. Irvin G. Stiglitz of M.I.T. Lincoln Laboratory.